LAWRENCE
LIVERMORE
NATIONAL
LABORATORY

LLNL-JRNL-654108

# Symmetry and correlations underlying Hidden Order in URu2Si2

N. P. Butch, M. E. Manley, J. R. Jeffries, M. Janoschek, K. Huang, M. B. Maple, A. H. Said, B. M. Leu, J. W. Lynn

May 8, 2014

Physical Review B

## Disclaimer

This document was prepared as an account of work sponsored by an agency of the United States government. Neither the United States government nor Lawrence Livermore National Security, LLC, nor any of their employees makes any warranty, expressed or implied, or assumes any legal liability or responsibility for the accuracy, completeness, or usefulness of any information, apparatus, product, or process disclosed, or represents that its use would not infringe privately owned rights. Reference herein to any specific commercial product, process, or service by trade name, trademark, manufacturer, or otherwise does not necessarily constitute or imply its endorsement, recommendation, or favoring by the United States government or Lawrence Livermore National Security, LLC. The views and opinions of authors expressed herein do not necessarily state or reflect those of the United States government or Lawrence Livermore National Security, LLC, and shall not be used for advertising or product endorsement purposes.

# Symmetry and correlations underlying Hidden Order in $URu_2Si_2$

Nicholas P. Butch,[1,2,3,*] Michael E. Manley,[4] Jason R. Jeffries,[3] Marc Janoschek,[5,6] Kevin Huang,[6] M. Brian Maple,[6] Ayman H. Said,[7] Bogdan M. Leu,[7] and Jeffrey W. Lynn[2]

[1] *Center for Nanophysics and Advanced Materials, Department of Physics, University of Maryland, College Park, MD 20742*
[2] *NIST Center for Neutron Research, National Institute of Standards and Technology, 100 Bureau Drive, Gaithersburg, MD 20899*
[3] *Lawrence Livermore National Laboratory, 7000 East Ave., Livermore, CA 94550*
[4] *Oak Ridge National Laboratory, Oak Ridge, Tennessee 37831*
[5] *Los Alamos National Laboratory, Los Alamos, New Mexico 87545*
[6] *Department of Physics, University of California - San Diego, 9500 Gilman Drive, La Jolla, CA 92093*
[7] *Advanced Photon Source, Argonne National Laboratory, 9700 S. Cass Ave., Argonne, IL 60439*

(Dated: April 29, 2014)

The organization of correlated electrons in the Hidden Order (HO) phase of intermetallic $URu_2Si_2$ is a longstanding mystery. In this work, we study the electronic symmetry by mapping the lattice and magnetic excitations via inelastic neutron and x-ray scattering measurements in the HO and high-temperature paramagnetic phases. The HO phase emerges from a highly-directionally correlated paramagnetic phase that gives rise to anisotropic bulk properties. However, at all temperatures the excitations respect the zone edges and symmetries of the body-centered tetragonal paramagnetic phase, showing no signs of reduced lattice symmetry even in the HO phase. Moreover, the magnetic excitations trace the experimentally determined Fermi surface, and their evolution with temperature marks them as a direct signature of itinerant correlations. At the HO phase transition, the opening of energy gaps in the magnetic excitations reflects a change in the hybridization of the many-body correlated state.

Subject areas: Condensed Matter Physics, Strongly Correlated Materials, Magnetism

The underlying cause of a large entropy change at the Hidden Order (HO) transition temperature $T_{HO}$ = 17.5 K in $URu_2Si_2$ remains a mystery, despite many experimental and theoretical developments over more than a quarter century since its discovery [1–3]. The HO phase develops out of a complicated correlated electronic paramagnetic state built of interacting itinerant and localized uranium $f$-electron states. Moreover, it is unstable to an unconventional superconducting ground state. Identifying the HO parameter is among the most persistent and thought-provoking challenges facing condensed matter physics.

Experiments cannot conclusively identify a symmetry-breaking order parameter to account for the configurational change measured at the ordering temperature. The shape of the specific heat anomaly at $T_{HO}$ resembles the second-order Bardeen-Cooper-Schriefer superconducting transition, suggesting that an energy gap is created in the itinerant electron states [1, 2]. Spectral gaps are also observed in optical [4] and electron tunneling measurements [5–7], but these features develop at temperatures greater than $T_{HO}$, so it is likely that these gaps are associated with the development of local-itinerant electron correlations starting as high as 80 K. As to the nature of the order parameter, early neutron diffraction identified A-type antiferromagnetic (AFM) order below $T_{HO}$, but the small measured moment is incompatible with the large entropy release [8]. This sample-dependent moment actually arises due to defects [9, 10] that stabilize puddles of an inhomogeneous large-moment antiferromagnetic (AFM) phase [11, 12], which evolves into a bulk phase above a first-order phase transition at 0.8 GPa [13]. Any ordered moment intrinsically associated with the HO phase must be very small [14–16]. Similarly, x-ray diffraction measurements indicate that there is no change in crystal symmetry through $T_{HO}$ [17]. Nonetheless, experiment [18, 19] and theory [20–24] continue to suggest that the HO transition involves a reduction of lattice symmetry.

To look for signs of incipient symmetry-breaking, we measured the magnetic and lattice excitations of $URu_2Si_2$ in the HO and paramagnetic phases to energies as high as 30 meV across much of reciprocal space. Temperature-dependent magnetic scattering is sensitive to the development of electronic correlations below 80 K, which yield overdamped paramagnetic excitations across reciprocal space. Anisotropy is clearly evident in the in-plane magnetic scattering intensity as well as the dispersion of the lowest energy optic phonon modes. The HO phase emerges out of a correlated electron state with an underlying directional preference, which is likely inherited from the anisotropy of localized uranium $f$-orbitals.

However, our study demonstrates that neither the magnetic nor lattice excitations violate the symmetry of the high-temperature paramagnetic phase, contrary to prevailing ideas that the HO phase shares the broken lattice symmetry of the pressure-induced AFM phase. Our data are inconsistent with theories invoking a primary uranium-based antiferromultipolar order parameter. The magnetic excitations follow the shape of the

experimentally-determined Fermi surface [25], indicating that they are direct signatures of hybridization with the $f$-states. Our results neatly demonstrate the dual itinerant/local electron nature of the HO phase and the correlated electron state from which it emerges.

## Experiment

Measurements were performed on a 7 g single crystal of $URu_2Si_2$ that was synthesized via the Czochralski technique in a continuously-gettered, tetra-arc furnace and subsequently annealed. Inelastic neutron scattering measurements were carried out on the BT-7 thermal triple axis spectrometer at the NIST Center for Neutron Research [26]. Temperature was controlled by a closed-cycle refrigerator. Inelastic scans were measured at constant wavevector $Q$ and varying energy transfer $E$. Typical scattering conditions were 50' - 25' - 50' - 120' collimation with 14.7 meV final energy. Energy resolution was approximately 1.2 meV full-width-half-max at the elastic position. Data were collected in both $a-a$ (basal) plane and $a-c$ plane geometries. Polarized neutron scattering measurements were performed using a $^3$He-based apparatus [27] with open - 50' - 80' - 120' collimation, a vertical guide field, and 14.7 meV final energy. An initial flipping ratio of 60 was determined from the nuclear $(2,0,0)$ reflection.

Time-of-flight inelastic neutron scattering measurements were performed on the NG-4 disc-chopper spectrometer at the NIST Center for Neutron Research [28]. Temperature was controlled by a closed-cycle refrigerator. The instrument was run in low-resolution mode with incident energy 13.09 meV (wavelength 2.5 Å) and scattering in the $a-a$ plane. Data were collected over 180° of sample rotation. Energy resolution ranged from 0.77 meV at elastic scattering to 0.4 meV at 10 meV transfer. Data analysis was performed using the DAVE software suite [29].

Inelastic x-ray scattering measurements on a single crystal with lateral dimensions 0.3 mm and thickness 0.015 mm were carried out on the HERIX beamline at Sector 30 of the Advanced Photon Source using 23.7 keV incident energy photons, with an energy resolution of 1.5 meV. Approximate x-ray spot size on sample was $35 \times 15$ $\mu$m$^2$. A pressure of 2.0 GPa was applied via a diamond anvil cell using a 4:1 methanol/ethanol pressure medium, while temperature was controlled using a helium flow cryostat. Ruby fluorescence was used for manometry. Measurements were performed along the $(h,h,0)$ direction.

Throughout this paper, error bars associated with measurements correspond to one standard deviation unless otherwise noted. Error bars not plotted are smaller than the plotted points.

## Overview

A summary of the low-energy magnetic and lattice excitations in the HO phase, as determined by both neutron and x-ray scattering, is presented in Fig. 1. For orientation, a reciprocal space map of the body-centered tetragonal (BCT) lattice of $URu_2Si_2$ shows the Brillouin zone (BZ), and identifies the high-symmetry points and lines along which the dispersions have been plotted. Points of particular interest are BZ center $\mathbf{\Gamma}$, horizontal face center $\mathbf{X}$, vertical face center $\mathbf{Z}$ and horizontal edge center $\mathbf{\Sigma}$, as well as corners $\mathbf{Y}$ of horizontal zone faces. Historically, these reciprocal-lattice points have been labeled using a simple tetragonal (ST) coordinate system, such that $\mathbf{Z}$ = {1,0,0} and $\mathbf{\Sigma}$ = {$q_1$,0,0} where $q_1 = \frac{1}{2}(1 + \frac{a^2}{c^2}) \approx 0.6$. Note that the horizontal path $\mathbf{\Gamma}$-$\mathbf{\Sigma}$ extends to $\mathbf{Z}$, which sits on the vertical zone boundary between adjacent BZs that are offset along the $c$-axis. When discussing directions, we remain consistent with the literature and refer to the $a = (1,0,0)$ and $c = (0,0,1)$ axes of the ST unit cell with lattice parameters a = 4.13 Å and c = 9.58 Å.

Figure 1 shows the reduced wavevector $q$ and $E$ dependence of the excitations in $URu_2Si_2$. The in-plane directions are designated $a_1$ and $a_2$ to distinguish longitudinal from transverse polarization, respectively. Note that on the left side of the dispersion plot, $a_1$ rotates by 45° to remain parallel to the radial direction and maintain the conventional definition of longitudinal and transverse polarizations along the $\mathbf{\Gamma}$-$\mathbf{Z}$ and $\mathbf{Z}$-$\mathbf{X}$ directions, as indicated in the plot. Magnetic excitations are consistent with previous studies, and new branches have been identified along several previously unpublished directions, including $\mathbf{\Gamma}$-$\mathbf{X}$.

Given the complexity of the excitation spectra, we first address the magnetic and lattice excitations separately. Then we discuss the implications of these excitations to the thermodynamics, the electronic structure, and the symmetry properties and nature of the HO phase itself.

## Magnetic excitations

The most prominent features of the magnetic excitation spectrum are $E$ minima at the $\mathbf{Z}$ and $\mathbf{\Sigma}$ points of the BCT BZ. The former is commensurate with the crystal lattice, while the latter is incommensurate. The commensurate point corresponds to the AFM ordering vector and features the smallest energy gap. However, unlike typical low-$E$ transverse magnons, the magnetic excitations in $URu_2Si_2$ are longitudinal, with a spin orientation along the out-of-plane magnetic easy axis of the system. The analogy to magnons is ultimately challenged by the lack of magnetic order in the HO phase. Meanwhile, the magnetic excitations at $\mathbf{\Sigma}$ feature a larger energy gap, but its opening can quantitatively account for the entropy

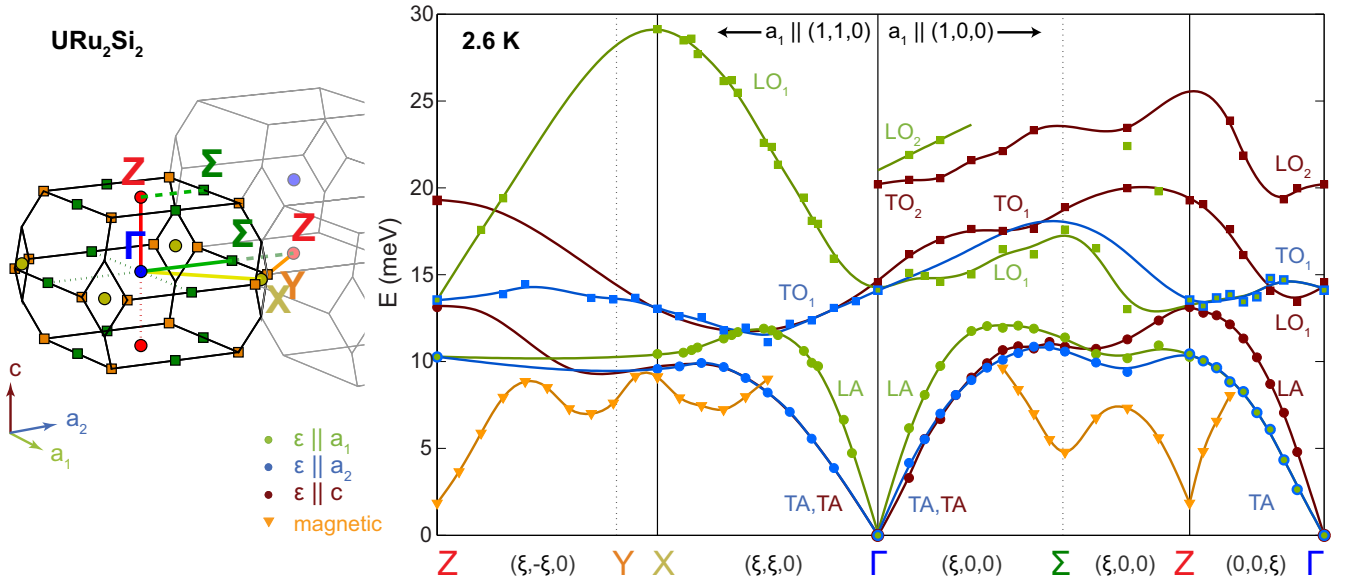


FIG. 1. Phonon and magnetic dispersions in the $URu_2Si_2$ hidden order phase. High-symmetry paths in the Brillouin zone of the BCT unit cell correspond to the wavevectors plotted on the right. Colors correspond to the phonon polarization $\varepsilon$ and shapes delineate different modes. The lowest-energy in-plane longitudinal optic $LO_1$ phonon modes are strongly anisotropic between the **Γ**-**X** and **Γ**-**Σ** directions. Magnetic excitations are delineated by orange triangles. A new branch of higher-energy magnetic excitations is identified along the **Γ**-**X** direction. Lines are guides to the eye. Displacements in reciprocal space $\xi$ are given in terms of reduced simple tetragonal coordinates. Longitudinal **Γ**-**X** phonons were measured at 4 K.

change at $T_{HO}$ [30]. Subsequently, several proposals have identified **Σ** with Fermi surface nesting, although conventional density wave order appears to be inconsistent with experiments [7, 31].

*The Hidden Order phase*

The measured magnetic excitations along important reciprocal space directions are shown in Fig. 2, in which a smooth extrapolation to a 12-15 meV intercept at **Γ** is included (dashed lines). Thus the spectrum is defined everywhere in reciprocal space, even though magnetic excitations are not observed experimentally above 10 meV. This picture represents a simple interpretation of the measured excitations, assuming that all should be treated as part of a continuous dispersion. The appreciable coverage of reciprocal space by our measurements allows a confident numerical interpolation of the dispersion over the entire BZ, from which a magnetic density of states (DOS) can be calculated, shown to the right of the dispersion in Fig. 2. The extrapolated higher-$E$ excitations do not contribute appreciably to the overall magnetic DOS because they occupy a small fraction of the BZ. For similar reasons, the low-$E$ excitations near **Z** also contribute negligibly to the magnetic DOS. Compared to the spin-wave model originally proposed by Broholm and coworkers [32], there are several differences. First, the experimental DOS from our measurement has a strong, relatively narrow peak at about 7 meV, which is in better agreement with that found in the real part of the optical conductivity [4], strengthening the argument that there is important spin-charge correspondence in $URu_2Si_2$. Second, there is no spectral weight above 10 meV in our measured data, and it is negligible in the extrapolation. For example, a smaller intercept at **Γ** would result in an area-conserving slight downward shift and modest increase in the higher-energy DOS that would not affect our conclusions. As Figure 3 shows, the measured magnetic excitations primarily have energies between 6 and 8 meV, which is not captured by the spin-wave model. Rather, this narrow bandwidth is most consistent with magnetic excitations deriving from a quasi-localized electronic state that disperses due to hybridization with itinerant electrons.

The magnetic dispersion in the HO phase is strikingly anisotropic in the tetragonal basal plane. It is mapped in Figure 3a, which is composed from the energies of maximum inelastic magnetic intensity determined from numerous constant-$Q$ scans and plotted in a symmetrized reduced zone scheme. Consistent with previous reports, the global minimum with a value of 1.8 meV is found at **Z**, while a broad local minimum with a value of 4.8 meV is centered at **Σ**. The local minimum at **Σ** is fairly sharp along the **Γ**-**Z** direction (see also Fig. 1), but its dispersion in the perpendicular in-plane **Σ**-**Y** direction is much weaker. This difference arises from BCT symmetry, be-

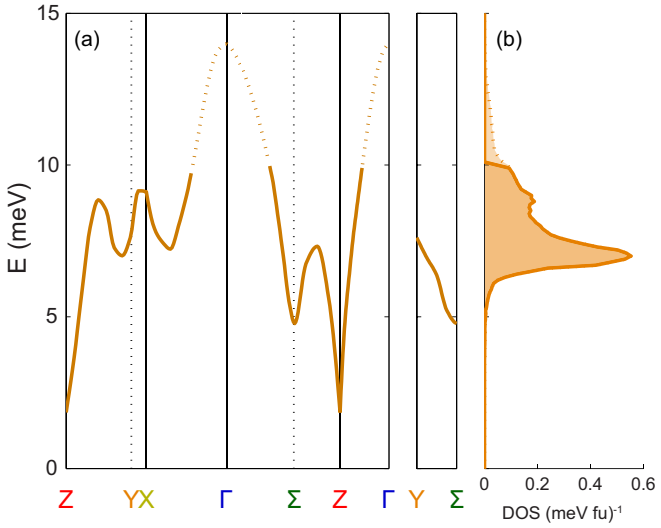


FIG. 2. Magnetic excitations in the HO phase. a) Dispersion of magnetic excitations at 2.6 K and b) corresponding magnetic density of states (DOS). At energies above 10 meV, the dotted lines represent smooth extrapolations towards **Γ**; no magnetic excitations are actually observed at these $q$. The narrow bandwidth of the excitations reflects their origin in a hybridized $f$-band.

cause **Σ** sits on the zone boundary (heavy black lines in Fig. 3) separating one BZ from the shared top/bottom face of its immediate neighbors (see Fig. 1 for a 3D view). Thus the perpendicular dispersion tracks a zone edge mode extending to the square corner **Y**. To quantify the asymmetry, we treat the dispersion as purely quadratic near **Σ** for simplicity: the coefficients are $523 \pm 27$ meV-Å$^2$ towards **Γ** and $93 \pm 2$ meV-Å$^2$ towards **Y** (Fig. 2). There is no symmetry relating the **Σ**-**Γ** and **Σ**-**Z** directions, but the excitations are roughly symmetric within 0.1 reciprocal lattice units (r.l.u.) $\approx 0.15$ Å$^{-1}$ of **Σ**. The magnetic excitations thus form a symmetric trough along the **Σ**-**Y** zone edge. This trough remains recognizable, although shallower and having higher $E$, halfway between **Σ** and **Y** (see Fig. 4b for detail). Near the corner **Y**, the trough turns slightly inward toward **Z**, and the local minimum sits 0.15 r.l.u. off of **Y**. This structure remains well-defined, with the sharpest excitations at the trough minimum, as seen in Fig. 4a,b. As the excitations leave the vicinity of the zone edge, they broaden and become poorly defined, except in the vicinity of the **X** point.

The magnetic dispersion in the vicinity of **X** has received little attention since early work by Broholm et al [32]. Approaching **X**, the magnetic excitation energy increases, but here the excitations remain well-defined. The path **Y**-**X** traverses a zone edge, tracing a line across a face shared by adjacent BZs. In the perpendicular direction **X**-**Γ**, the magnetic excitations disperse initially downward and then upward in $E$, hitting a local mini-

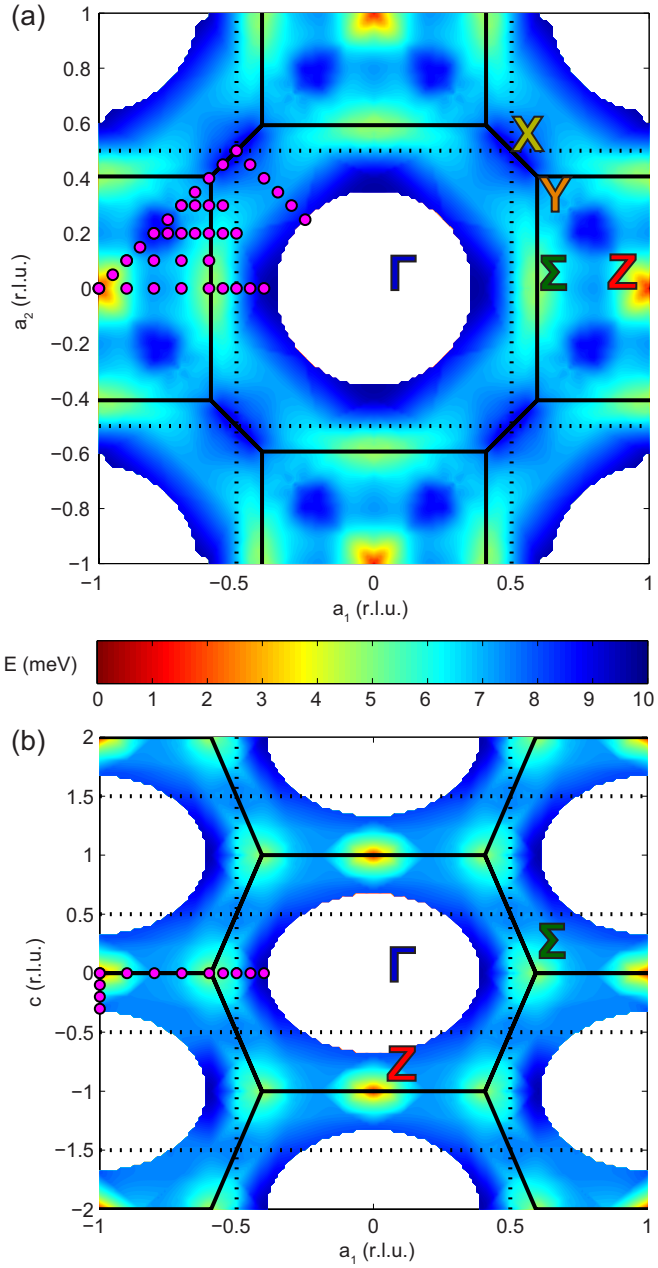


FIG. 3. Magnetic dispersion in the HO phase in a) the basal plane and b) the $a$-$c$ plane. The energies are identified in the color bar. Minima exist at the **Z** and **Σ** points and the magnetic excitations are experimentally unobserved in proximity to the **Γ** point. In a) it is apparent that the excitations near the **Z** and especially the **Σ** minima disperse anisotropically. In b) the dispersion is more circular or ellipsoidal about the minima. Along both projections, the magnetic excitations trace the boundaries of the BCT reciprocal lattice (in heavy black). For reference, dotted lines represent the ST lattice of the AFM unit cell. Magenta points denote the $q$ at which the excitations were measured. Data were tesselated to create the 2D plots and $c$-axis dispersion data near **Σ** from Ref. [30] were used to fill in figure b). Note that these are *not* intensity plots.

mum approximately $\frac{1}{3}$ of the way towards $\mathbf{\Gamma}$ (Fig. 4c). The magnetic nature of these excitations, which are similar in $E$ to the phonons at $\mathbf{X}$ has been confirmed via polarized neutron scattering (Fig. 5). These data distinguish the magnetic and lattice excitations in Fig. 4c, and are consistent with the inelastic x-ray scattering discussed later. The magnetic excitations become poorly defined farther away from the zone boundary and are impossible to track past a point halfway toward $\mathbf{\Gamma}$, where their $E$ becomes comparable to that of the phonons (Fig. 1,4c). A similar intensity loss is found along the $\mathbf{\Gamma}$-$\mathbf{\Sigma}$ and $\mathbf{\Gamma}$-$\mathbf{Z}$ branches (Fig. 1), such that the dispersions near $\mathbf{\Gamma}$ in any direction remain experimentally undefined. The intensity loss of the magnetic scattering at small $q$ might be due to an AFM-like structure factor, with the caveat that there is no actual long-range AFM order to cause this. A second possibility is strong damping from magneto-acoustic coupling where the phonon and magnon $q$ and $E$ become comparable (Fig. 1) leading to increased scattering that shortens the magnetic excitation lifetimes. Alternatively, as 10 meV $k_B \approx 120$ K (where $k_B$ is the Boltzmann constant), this $E$ scale might constitute a cut-off for excitations of the correlated electron state. Yet, the magnetic excitations seem to approach 10 meV without disappearing at other $q$, including near $\mathbf{X}$. Before addressing this discrepancy, we first focus on the magnetic excitations near $\mathbf{Z}$.

The $\mathbf{Z}$ point has long been a focus of study. It is a marker of broken lattice symmetry because $\mathbf{Z}$ becomes equivalent to $\mathbf{\Gamma}$ when BCT symmetry is reduced to ST, as is known to occur in the pressure-induced AFM phase. Even though the presence of long-range magnetic order in the HO phase is now in doubt, a lattice-symmetry reduction is still widely suspected as a feature of the HO transition. The $\mathbf{Z}$ point also stands out because it is the location of the smallest energy gap. The excitations at $\mathbf{Z}$ are intense and long-lived, as noted in many previous studies [30, 32, 33]. However, the excitations broaden and become hard to track beyond only about 0.1 r.l.u. away. Such an intensity drop is clearly observed along the $\mathbf{Z}$-$\mathbf{X}$ direction (Fig. 4a). To better visualize this intensity drop and to demonstrate that it is not simply the result of lifetime broadening, the integrated intensity is plotted in Fig. 4d. Along the $\mathbf{Z}$-$\mathbf{X}$ cut (path a) the magnetic intensity clearly drops by an order of magnitude within a small $q$-window about $\mathbf{Z}$. Continuing towards $\mathbf{Y}$ the intensity once again increases until it reaches a maximum when it joins the trough near the BZ edge. These variations suggest that the magnetic excitations at $\mathbf{Z}$ are distinct from those at the zone boundary [30]. Indeed, the excitations respond differently to experimental tuning: applied pressure opens the energy gap at $\mathbf{\Sigma}$ and closes the gap at $\mathbf{Z}$ [33], and Re substitution selectively suppresses the excitations at $\mathbf{Z}$ [34].

The excitations in the $a-c$ plane are shown in Fig. 3b. They are consistent with earlier inelastic neutron data

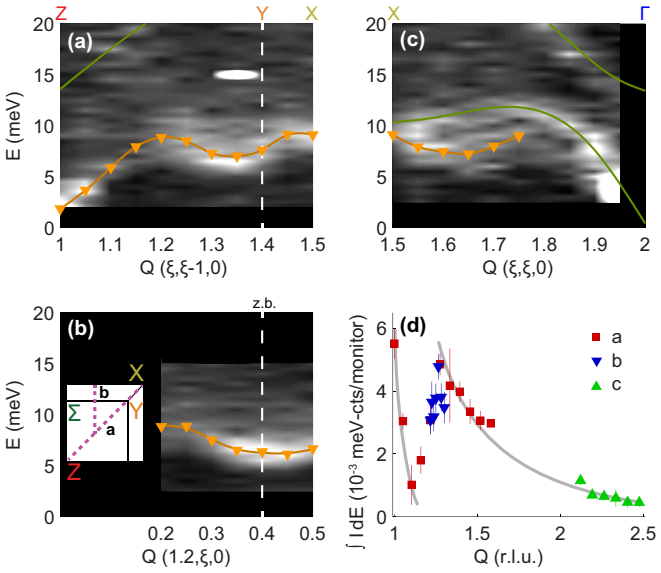


FIG. 4. Intensity variation of the magnetic excitations along selected basal-plane directions in the HO state as measured via inelastic neutron scattering. Intensity contours a)-c) were built from $E$ scans at constant $Q$. a) Along the $\mathbf{Z}$-$\mathbf{X}$ line the most intense magnetic scattering is observed in the vicinity of local minima in the dispersion. b) A 45° cut away from path a) yields an intense local minimum near the zone boundary. c) The magnetic excitations along $\mathbf{X}$-$\mathbf{\Gamma}$ are almost degenerate with the LA phonon but have a local minimum. Orange triangles and lines correspond to magnetic excitations, while green lines correspond to phonons. d) The integrated intensities of the magnetic excitations in a)-c) show that along the $\mathbf{Z}$-$\mathbf{X}$ line that there is a precipitous drop in intensity quite close to the $\mathbf{Z}$ point, implying that the AFM dispersion is distinct from the $\mathbf{\Sigma}$-$\mathbf{Y}$ zone edge modes. Maximum intensities of a) and b) are comparable, but c) is much less intense. Gray lines are guides to the eye. Uncertainties derive from least squares fits of Lorentzian lineshapes to magnetic peaks.

[30], but the reciprocal space dimensions are shown to scale to highlight the isotropy of the excitations. We first focus on the $\mathbf{\Sigma}$-centered dispersion, which is roughly isotropic in the $a-c$ plane, in contrast to the anisotropy in the basal plane. When compared to an overlay of the BCT reciprocal lattice (black lines), the correspondence between the lattice edges and the magnetic excitations is obvious, as the $\mathbf{\Sigma}$-centered excitations are stacked in a vertical zig-zag. We emphasize that these excitations do not respect ST symmetry. Focusing on the $\mathbf{Z}$-centered excitations, in this view it is clear that they disperse more strongly along $c$ than $a$. The magnetic excitations of the HO phase are confined to the BCT BZ faces. The trough structures are reminiscent of the scattering expected of previously proposed orbital currents [35] that were experimentally discounted [36], but they are not circular and they are well removed in $E$ from the elastic line. This coincidence is likely accidental because, as we discuss later, the excitations bear a remarkable similarity to

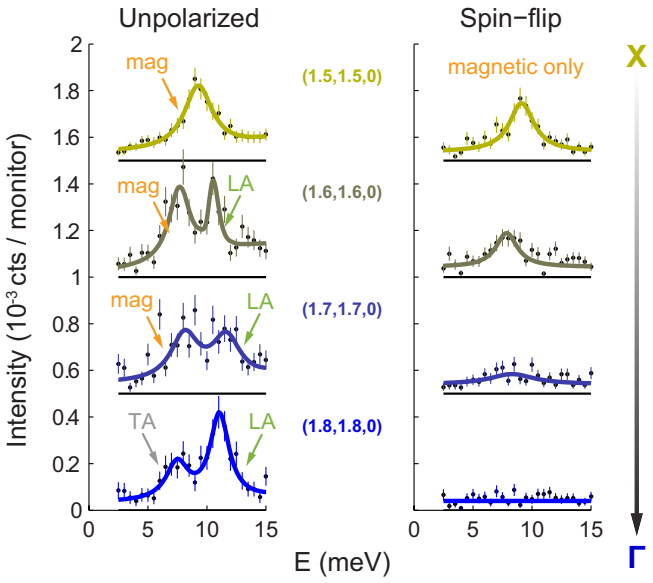


FIG. 5. A comparison of unpolarized and polarized inelastic neutron scattering along the **X**-**Γ** direction. In the unpolarized neutron data, both LA phonons and magnetic excitations are seen. The lower-energy mode at $Q = (1.8, 1.8, 0)$ is a forbidden $c$-polarized TA phonon. Only coherent magnetic scattering causes a reversal of the neutron spin, and here the spin-flip polarized scattering clearly shows a well-resolved peak at **X** that disperses and weakens approaching **Γ**, demonstrating that this scattering is purely magnetic in origin.

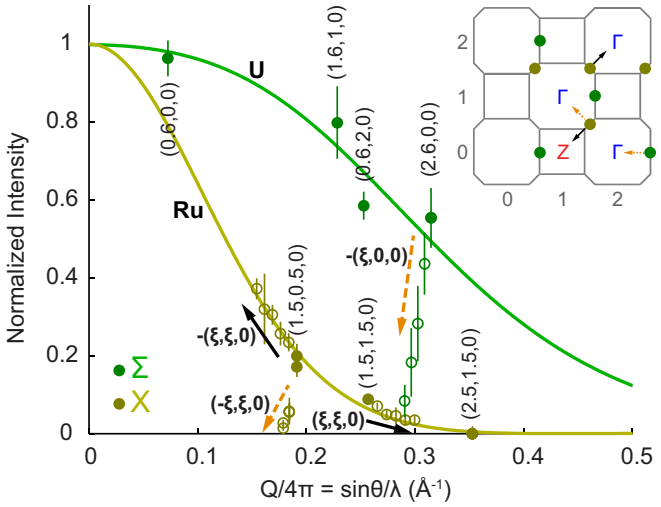


FIG. 6. Inelastic magnetic form factor for excitations at **X** (9.1 meV) and **Σ** (4.8 meV) and related points measured via inelastic neutron scattering. The **Σ** intensities at this energy have relatively weak $Q$-dependence consistent with well-localized $5f$ moments, whereas the intensities at **X** have a strong $Q$-dependence, reflecting the much larger spatial extent of these correlated electrons. The intensities along the (ξ,ξ,0) direction (open circles, solid arrows) collapse to a common curve. In contrast, the intensities along perpendicular directions (dashed arrows) decrease dramatically faster than either form factor, demonstrating the additional presence of a magnetic structure factor that modulates the intensities due to interference in the scattering. Filled circles correspond to symmetrically equivalent points at different $Q$, whereas open circles correspond to deviations towards high-symmetry points indicated near the corresponding arrows. For reference, the **Σ** and **X** intensities are fit to U and Ru form factors, respectively. Error bars represent least-squares fitting uncertainties.

the electronic structure.

*Magnetic anisotropy*

To assess the spatial distribution of the magnetic moments in $URu_2Si_2$, we measured the form factor of the inelastic magnetic scattering, the square of which modulates the intensity. Earlier polarized neutron diffraction measurements in the paramagnetic phase at a relatively high temperature of 60 K showed that the basal-plane magnetic form factor is isotropic, with values consistent with scattering from either free-ion $U^{3+}$ or $U^{4+}$ moments, which are experimentally difficult to distinguish [37]. The basal plane is perpendicular to the magnetic easy axis, whose bulk magnetic susceptibility also reflects the full free-ion $U^{3+}$ or $U^{4+}$ moment at high temperatures [1]. Although the susceptibility deviates substantially from a Curie-Weiss law below 100 K, the previous form factor measurement implies that the electronic configuration remains similar to that of a free uranium ion.

Interestingly, our data show that this isotropy does not persist into the HO phase. At low temperatures the form factor of the magnetic excitations exhibits a marked anisotropy between the **Γ**-**Σ** and **Σ**-**X** directions. Figure 6 shows that the $Q$-dependence, denoted as $sin\theta/\lambda$, of the integrated magnetic scattering intensity at the **Σ** points (solid green circles) varies weakly over the measured range of reciprocal space, consistent with scattering from $U^{3+}$ or $U^{4+}$. Because the real-space magnetization density is the Fourier transform of the magnetic form factor, the gentle $Q$-dependence is consistent with spatially localized $f$-states and corroborates earlier conclusions based on both magnetic diffraction[32] at **Z** and inelastic magnetic scattering at **Σ** [36]. In contrast, the magnetic integrated intensity at the **X** points (solid gold circles) reduces much more quickly at larger $Q$, essentially disappearing by $Q = (2.5, 1.5, 0)$. This sensitive $Q$-dependence indicates a spatially extended magnetization density, and is slightly sharper than the form factor of $Ru^{+}$. Thus along certain directions, the magnetization density, which stems from the $f$-states, is actually more reminiscent of larger $d$-states.

Magnetic form factor anisotropy is observed in transition metal elements and alloys [38], arising from the re-

distribution of electrons due to itineracy, bonding [39], or crystal field effects. Although form factors are typically studied via magnetic diffraction, looking at the inelastic magnetic scattering has, for example, yielded insight into electron hybridization in cuprates [40]. In the case of $URu_2Si_2$, the form factor anisotropy is a characteristic of the magnetic excitations, which are strongly temperature dependent. The anisotropy likely emerges at temperatures lower than 60 K [37], and is a signature of the electronic correlations. Retreating from the **X**-point excitations along $(\xi, \xi, 0)$ (Fig. 6 open gold circles), the intensities fall on the same form factor curve, as would be expected of paramagnetic excitations, a detail that is consistent with the lack of static dipolar order in the HO phase.

Yet other, additional intensity modulation must be associated with the HO phase itself. It is relatively straightforward to find counterexamples of the aforementioned paramagnetic form factor along other directions, as shown in Fig. 6: along the paths (-$\xi$,$\xi$,0) away from **X**, and (-$\xi$,0,0) away from **Σ**, which both feature decreasing intensity but increasing $Q$. This behavior indicates that the magnetic intensity in the HO phase is modulated by an additional effective dynamic *structure* factor, due to long-range correlations that are typically a feature of a magnetically ordered phase. As with magnetic form factors, magnetic structure factors are often experimentally determined through elastic magnetic diffraction, which is impossible in this case because there is no intrinsic dipolar magnetic structure in the HO phase. Even so, it is possible to consider the simple AFM structure stabilized by pressure, whose spatial symmetry is assumed by many to be shared with the HO phase. The experimentally-determined intensity modulation, particularly the rapid decrease near **Z** (Fig. 4) and increase near **Σ** and **Y** is inconsistent with that simple AFM structure.

*Temperature dependence*

Upon cooling, hybridization increases between the localized uranium $f$-electron states and the itinerant conduction electrons, introducing new states into the conduction band. In the bulk properties, this behavior is evident over the range of 60-80 K, where the electrical resistivity and magnetic susceptibility have their maximum values [1, 3], as does the $\frac{1}{2}(c_{11}-c_{12})$ elastic constant [41]. This temperature range is higher than that associated with the opening of a gap in the electronic DOS [7] in the paramagnetic phase at approximately 30 K [4, 6], although this does not preclude a common physical origin. In fact magnetic excitations have been tracked to temperatures as high as 100 K via inelastic neutron scattering [30, 32].

Our measurements demonstrate that at high temperatures, the magnetic spectrum consists of overdamped

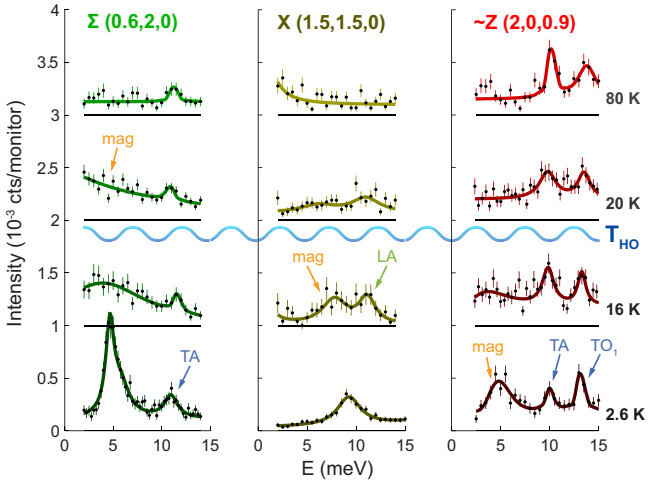


FIG. 7. Temperature dependence of the magnetic excitations at different points illustrates that high-temperature paramagnetic excitations exist across the BZ and evolve similarly as a function of temperature. At 80 K, the hybridization of $f$-electrons is apparent at the **X** point where overdamped magnetic excitations mask weak scattering from the LA phonon. Upon cooling, low $E$ excitations develop and narrow into peaks as $T_{\rm HO}$ is crossed. The higher-energy excitations are phonons, as indicated. The LA phonon at **X** is only resolved at intermediate temperatures.

modes situated across much of the Brillouin zone, not just at select locations in reciprocal space such as **Σ** [30]. A comparison of the temperature dependence of the inelastic neutron scattering data at different parts of the BZ at 80 K and below is shown in Fig. 7. At **Σ**, the strong and well defined magnetic excitation in the HO phase becomes severely broadened just below $T_{\rm HO}$ and quasielastic above. Similar behavior is also clearly observed at **Z**; due to the much smaller minimum energy gap, a proximate $Q$ point is shown in Fig. 7 to emphasize the temperature evolution, although intensity at low $E$ is significantly lessened (compare to the intensity at **Z** in Fig. 8). At the **X** point, a prominent low temperature peak splits in two upon warming. This seemingly unusual behavior is the result of an accidental near-degeneracy of the magnetic excitation (Fig. 5) and the LA phonon at low temperatures. Upon warming, the magnetic excitation broadens and moves to lower energy, while the phonon does not shift in energy. However, the phonon is relatively broad, and cannot be resolved in the 80 K data, which hints that it is also affected by the electron correlations. As we discuss below, this phonon is well-resolved in the inelastic x-ray scattering data at both high and low temperatures. This fact suggests that **X** is important to electron hybridization, and the temperature-evolution of the magnetic scattering there is consistent with an energy gap opening at temperatures greater than $T_{\rm HO}$ - note that at 20 K the magnetic peak is already centered

at 6 meV, although it is very broad. Broad quasielastic magnetic scattering is also observed along the **X**-**Γ** direction (not shown).

The character of the magnetic scattering is well demonstrated by time-of-flight inelastic neutron measurements, as shown in Fig. 8. Figure 8a) shows a contour plot of the scattering integrated from 2-8 meV at 25 K, well above $T_{\rm HO}$. The magnetic excitations strikingly trace the BCT BZ boundary, overlaid on the plot. Figures 8b-d show the $E$-dependence along high-symmetry cuts, in which the magnetic excitations appear as vertical stripes sharply defined in $Q$ at vectors **Σ**, **X**, **Y**, and **Z**. Most easily discernable in the intense scattering at **Σ**, scattering at this temperature is consistent with overdamped quasielastic diffusive excitations. Note that the excitations about **Σ** are extended along the BZ edge, consistent with the elongated shape of the dispersion in the HO phase (Fig. 3). Below $T_{\rm HO}$, these excitations become gapped, well-defined, and dispersive (Fig. 8f-h). The gapping occurs at multiple points in the BZ, indeed wherever magnetic scattering is observed. Nonetheless, the magnetic excitations continue to clearly trace the BCT BZ boundary, as shown in Fig. 8e, showing no evidence of spatial symmetry breaking. In addition, the separation between the scattering centered at **Z** and the trough is quite marked, again pointing to their disparate natures. A complete set of 0.2 meV $E$ slices from 2-8 meV is available in the Supplemental Online Material.

It has been argued that the gapping of the paramagnetic excitations in the vicinity of **Σ** by the HO transition can account for the entropy change at $T_{\rm HO}$ [30]. Although excitations in the $a$-$c$ plane appear localized about **Σ**, this model does not take into account the magnetic in-plane excitations away from **Σ**. Our data show that the magnetic dispersion evolves from overdamped fluctuations across the BZ, which means that many more magnetic states are gapped by the HO transition. Although the gapping of the magnetic excitation spectrum remains the most likely explanation for the entropy change at $T_{\rm HO}$, a complete accounting awaits the detailed temperature dependence of the entire magnetic dispersion, requiring precise measurements across reciprocal space.

### Phonons

The crystal lattice plays a seemingly passive role, showing no signs of broken symmetry in the HO phase [17]. Meanwhile, the excitation spectrum of the crystal lattice is poorly characterized beyond small $Q$. The energies of Raman-active optic phonons show minimal temperature dependence but signs of low-temperature electron-phonon coupling [42, 43]. Ultrasound studies, which probe the very low-$E$ acoustic phonons, show tendencies toward symmetry-breaking: softening is observed in a volume-conserving, symmetry-breaking mode below 70 K [41], and this softening disappears when high field destabilizes the HO phase [44]. There is also an increase in thermal conductivity at $T_{\rm HO}$ [45] that has been argued to arise from the electrostatic coupling of the HO parameter to the lattice [46]. Such coupling suggests that the phonons might display the in-plane magnetic and electronic anisotropy inferred from recent torque magnetometry [19] and cyclotron resonance measurements [47].

An evaluation of the low-energy phonon dispersions (Fig. 9) yields no signs of broken symmetry. Phonons propagating in the basal-plane can have longitudinal and transverse in-plane polarizations, denoted $a_1$ and $a_2$. For phonons propagating along the $c$-axis, the two transverse $a$ polarizations are degenerate by tetragonal symmetry: note the transverse acoustic TA and transverse optic $\rm TO_1$ phonons. Any lifting of this degeneracy due to dynamic symmetry breaking, say towards an orthorhombic distortion, is not observed. Born-von Karman force-constant modeling can reproduce the acoustic modes using a simplified BCT crystal consisting of only one uranium atom and 5 force constants. The success of this simple model implies that unconventional electronic or magnetic coupling are not required to explain the curvature of the acoustic dispersions, and based upon the model we conservatively interpolate the **Z**-**X** acoustic modes, which were not experimentally observed (Fig. 1). It is also worth noting that there is no obvious anomalous behavior in the acoustic modes that might suggest strong magnetoelastic coupling.

The lowest-energy optic $\rm O_1$ phonons intersect the zone center **Γ** at 14 meV, corresponding to the $a$-polarized infrared-active mode [4]. Of particular note is the directional sensitivity of longitudinally-polarized optic $\rm LO_1$ modes, which is readily apparent via a comparison of the two high-symmetry basal-plane directions **Γ**-**Σ** and **Γ**-**X** that are rotated with respect to each other by 45° (Fig. 9). The upward-dispersing **Γ**-**X** branch was originally difficult to identify in neutron scattering measurements, and was confirmed across several BZs via inelastic x-ray scattering (Fig. 10) that is sensitive to lattice, but not magnetic, excitations. Although it disperses strongly, the $\rm LO_1$ mode lacks any notable temperature or pressure dependence, indicating that it does not play an important role in the development of electronic correlations or the ordered phases. A similar steep dispersion is observed in $\rm UO_2$ [48], which results from the large mass ratios of the constituent elements.

At slightly higher energies, the $\rm O_2$ phonons include the Raman-active 20 meV excitation with $\rm B_{1g}$ symmetry [42]. From the literature, other known phonon modes at **Γ** are IR-active at 42.4 meV ($a$-polarized) and 47 meV ($c$-polarized) [4] and Raman-active at 55 meV ($\rm A_{1g}$ $c$-polarized) [42]. The broad $E$ range and well-separated phonon dispersions are attributable to the significant mass differences between Si, Ru, and U atoms. Although our measured phonon dispersions cover approximately

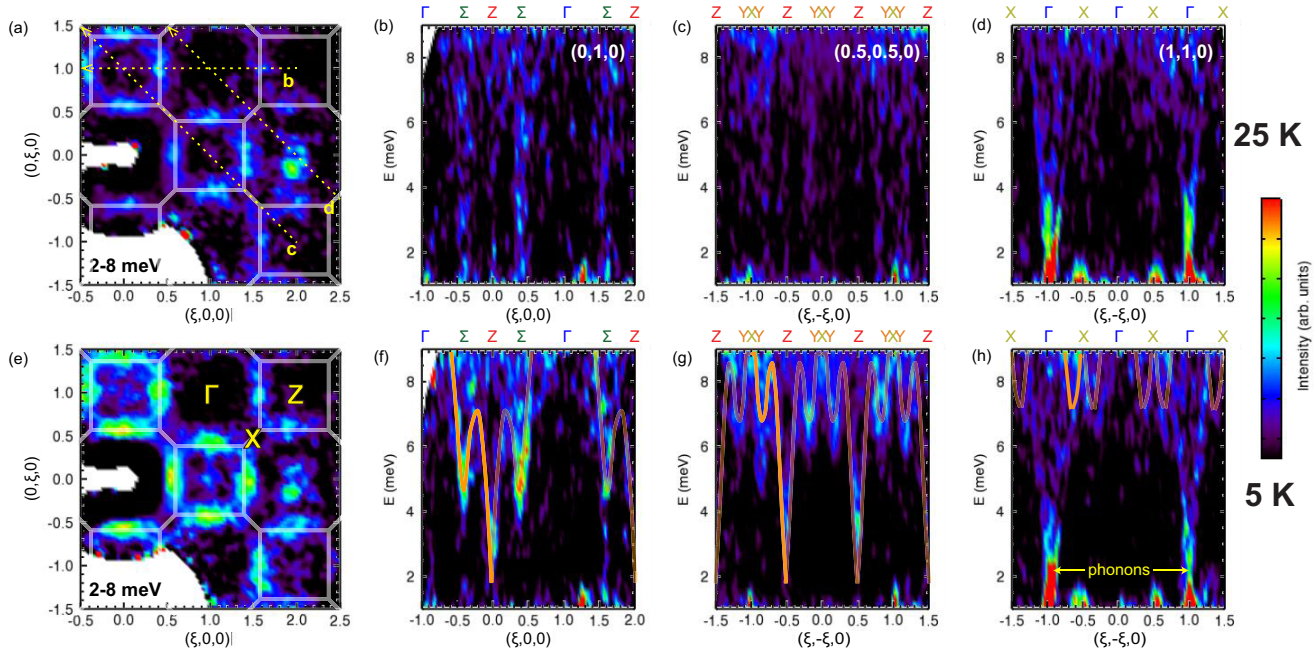


FIG. 8. Magnetic excitation spectrum above and below $T_{HO}$ as measured by time-of-flight neutron scattering. At 25 K, a) shows the intensity of excitations in the basal plane, integrated from 2-8 meV. The magnetic excitations trace the reciprocal lattice boundaries, overlaid in white. b-d) Energy dependence of magnetic excitations along selected cuts in the basal plane, with the constant $Q$-vector noted in the figure and intensity integrated over $\pm 0.05$ r.l.u. The magnetic scattering forms vertical stripes over the 1-9 meV energy range, indicative of overdamping. Specific points in reciprocal space are emphasized in b) **Σ**; c) **Z**, **Y**; and d) **X**. e-h) Same as a-d, but at 5 K. In the HO phase, the magnetic excitations are gapped and dispersive (compare to Fig. 2), but they respect the high-temperature BCT symmetry. Intensity diminishes at larger $Q$ due to the magnetic form factor. The magnetic dispersion in the HO phase is traced in orange. Intense excitations emanating from (2,0,0) and (0,2,0) are phonons. Intense blobs at 1.5 meV are due to scattering from the sample holder.

half of the known $E$ range of lattice excitations, the low-$E$ states are much more important to the thermodynamic and bulk properties of $URu_2Si_2$ because, obeying Bose-Einstein statistics, they are highly populated at low temperatures. We also point out that these phonon dispersions can be readily calculated from first-principles electronic structures and provide an important benchmark against which to compare new and existing calculations.

*Temperature dependence*

Although the superficial temperature dependence of the phonons (Fig. 9) is weak, notable details highlight important electronic interactions, particulary among the $c$-polarized phonons. First, LO phonon softening along **Γ**-**Z** is absent at 300 K, in contrast to the typical high-temperature phonon softening that arises due to thermal expansion. In the HO phase, in both the $c$-polarized $LO_1$ and $LO_2$ modes along **Γ**-**Z**, there is a shallow minimum 20-30% away from **Γ**. These features contrast with the relatively flat $TO_1$ dispersion at the same temperature. This low-temperature phonon softening at localized $q$ is a sign of electronic interactions and it is compelling that at least 2 optic modes having different symmetries are affected at the same $q$. In analogy to the classic case of chromium [49], this phonon softening could be associated with the opening of an energy gap in the electronic DOS, as observed in IR [4] and tunneling spectroscopy measurements [6].

Along the same phonon polarization branch, the $LO_1$ modes along **Γ**-**Σ** exhibit an extreme temperature dependence. The $TO_1$ $c$-polarized mode is much softer at 300 K than at 2.6 K (Fig. 9). This high temperature softening results in the inversion of the $TO_1$ mode with respect to the $LO_1$ mode along **Γ**-**Σ**. This suggests that temperature-dependent electron-phonon interactions preferentially play out along the **Γ**-**Σ** direction. It may be significant that softening occurs over a broad range of **Γ**-**Σ** wavevectors, differing from chromium, in which phonon softening is found at very specific $q$ related to the electronic Fermi surface [49].

One case of softening with increasing temperature is evident near the **Z** point, which occurs in the $a$-polarized TA phonons. At 300 K, these show an $E$ drop before the zone edge is reached as well as along the zone boundary **Σ**-**Z**. By 80 K, the dispersion is similar to that observed in the HO phase. The measured difference of

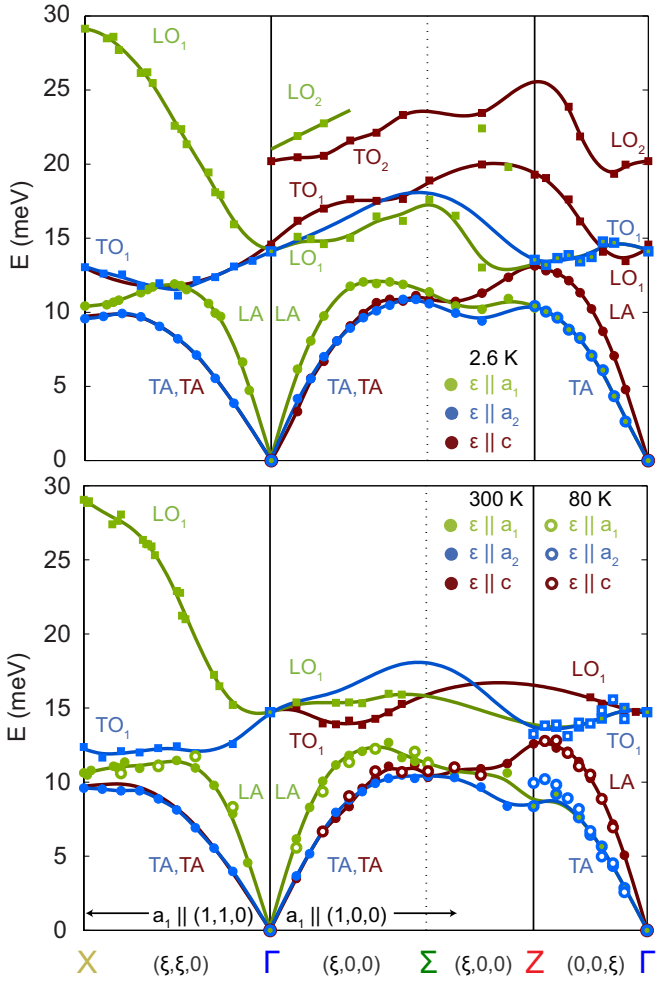


FIG. 9. Phonon dispersions at different temperatures. The high-temperature dispersions are largely similar to those in the HO phase. However, there are some notable exceptions. A dramatic difference in the 2.6 K data is that the low-lying $c$-polarized $TO_1$ mode lies at lower $E$ than the $LO_1$ mode along **Γ-Σ** and lacks the local minimum near **Γ** along the **Γ-Z** direction. Most features were determined via inelastic neutron scattering, but the $LO_1$ **Γ-X** mode was determined at 2.0 GPa using inelastic x-ray scattering.

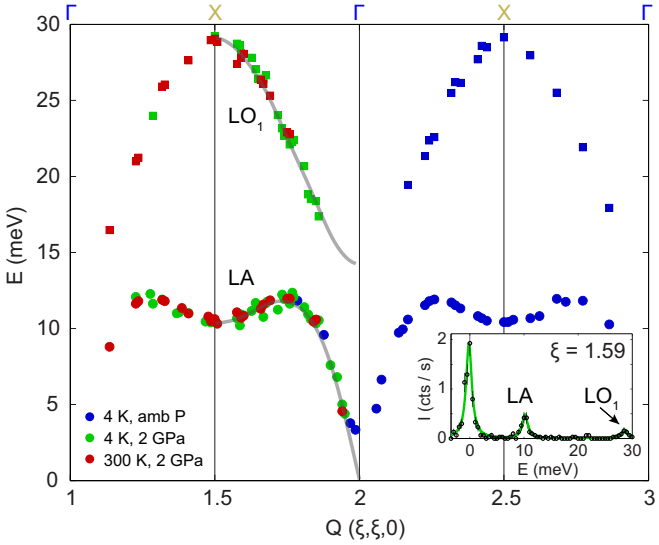


FIG. 10. Phonon dispersions determined using inelastic x-ray scattering clearly show the LA and $LO_1$ phonons along the **Γ-X** direction through several Brillouin zones. These dispersions are roughly independent of temperature and do not change with the modest applied pressure of 2.0 GPa that induces long-range AFM order. Lines are guides to the eye. The inset shows an example scan at constant $Q$, taken at 4 K and 2 GPa.

2 meV represents a large 20 % change. The expected relative change in $E$ is conventionally related to the relative change in lattice volume V by $\frac{\partial E}{E} = -\gamma \frac{\partial V}{V}$, where $\gamma$ is a Grüneisen parameter with a value of approximately 2. Between 300 K and 2.6 K, $\frac{\partial V}{V} \approx 10^{-3}$, from which we would expect a change smaller by 2 orders of magnitude. This large change hints that there are important changes in electronic structure near **Z** already occurring between 80 K and 300 K.

### Thermodynamics

Knowledge of the thermodynamic properties of the electronic and magnetic states in $URu_2Si_2$ is fundamental to their proper characterization, but has been a challenge because the phonon contribution is included in specific heat [1, 2] and DOS measurements [50] and must be accounted for properly. Our measurement of the low-$E$ phonon dispersions allows an accurate determination of the phonon contribution to the specific heat at low temperatures, and a confident subtraction from the experimentally measured specific heat. The result of this analysis is shown in Fig. 11. In Fig. 11a, the partial DOS of the acoustic (LA,TA) and optic ($LO_1$,$TO_1$) phonons is shown, from which the phonon specific heat curve in Fig. 11b (magenta) is calculated. The data points are taken from Reference [51]. Figure 11c shows the subtracted specific heat $\delta C$, divided by temperature, which is the electronic/magnetic contribution that accounts for the entropy change due to the HO transition. Calculated values for an effective electronic specific heat coefficient $\gamma_0 = 55$ mJ mol/K$^2$ in the HO phase and 160 mJ mol/K$^2$ above the transition. These values can be interpreted as indicating a large reduction of the electronic DOS at the Fermi level [2], or a removal of magnetic states [30]. The anomaly associated with the HO transition is well described by a form $\delta C \propto \exp\left(\frac{E_g}{k_B T}\right)$, where $E_g/k_B = 85$ K. This feature is often related to the opening of an energy

gap in the electronic DOS. The energy scale corresponds to that of the coherence temperature, or about $5 \times T_{\rm HO}$. A calculation of the entropy released by the transition, $\Delta S = \int dT(\frac{\delta C}{T} - \gamma_0)$, yields 1.1 J/mol K = 0.13 $k_{\rm B}$/fu, or only 20% of $R \ln 2$ expected from the lifting of degeneracy of a localized electronic doublet, which indicates that itinerant states must be involved in the transition. These values are in general agreement with early results [1, 2].

The measured phonon DOS further uncovers some interesting features in the temperature-dependence of the specific heat. The typical Debye approximation to the phonon specific heat is inaccurate here because there are significant deviations of the measured phonon DOS from the Debye model DOS at low $E$, and there is no reliable temperature range over which to fit the low-temperature approximate form of $C = \gamma T + \beta T^3$. There is particular uncertainty regarding the temperatures above the HO transition, where the $T^3$ approximation is well outside its range of applicability. The properly subtracted specific heat yields a slightly sublinear specific heat, seen as $C(T)/T$ having a negative slope, above the HO transition, as indicated in Fig. 11c. This behavior can be understood as the result of a decreasing electronic specific heat coefficient due to reduced $f$-electron hybridization as temperature increases. This interpretation is consistent with observation of other hybridization-related phenomena in this temperature range, in particular the closing of spectroscopic gaps [4, 6] above the HO transition temperature. It is also noteworthy that below 5 K, but above the superconducting transition, $C(T)/T$ also has a negative slope. This effect may be due to the effect of exotic superconducting fluctuations [52].

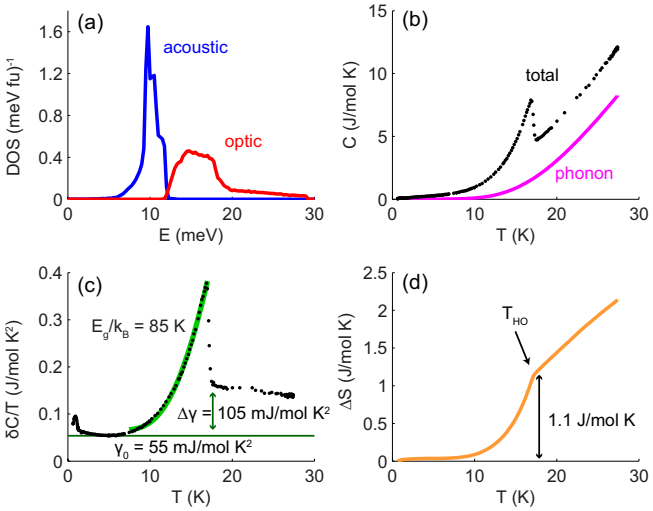


FIG. 11. Thermodynamic quantities derived from phonon dispersions. a) Density of states (DOS) for acoustic and lowest band of optic modes. b) Comparison of total experimental specific heat [51] and calculated phonon contribution. c) Difference of curves in b yields effective electronic and magnetic contributions to specific heat, shown here divided by temperature. The contribution in the paramagnetic phase actually decreases with increasing temperature. d) Calculated entropy in excess of the low-temperature $\gamma_0$ electronic contribution. The HO transition liberates 1.1 J/mol K, or 20% of $R \ln 2$.

### Relation to electronic structure

A challenge in the study of $URu_2Si_2$ is that fundamentals of the electronic structure, such as the number of $f$-electrons on the uranium ions, are still debated. Yet accurate knowledge of the electronic structure is central to understanding the phenomenology because bulk property and spectroscopic measurements all indicate that the Fermi surface changes as a function of temperature. A crucial detail is where in the BZ the Fermi surfaces sit: of particular historical concern has been the origin of the gap in the magnetic excitations at $\mathbf{\Sigma}$, which is often ascribed to Fermi surface nesting, and for which potential nesting vectors have been proposed [18, 22, 53, 54]. There have been many attempts to reconcile first-principles calculations [22, 55–57] with experimental angle-resolved photoemission spectrum (ARPES) [18, 25, 55, 58, 59].

The electronic structure near $\mathbf{Z}$ has been studied extensively by ARPES [18, 25, 55, 58–62]. A small hole pocket is centered on $\mathbf{Z}$ with an in-plane Fermi wavevector $k_F \approx 0.2$ Å$^{-1}$ $\approx 0.15$ r.l.u. A narrow band with $f$-character actually sharpens inside this pocket [58], consistent with expectations of $d$-$f$ hybridization in a periodic Anderson model [55]. In our data, this pocket covers a small range of $q$ over which anomalous TA phonon softening is observed near $\mathbf{Z}$ between 80 K and 300 K (Fig. 9), and this range of $q$ corresponds to the limits of the higher-intensity excitations centered on $\mathbf{Z}$ in the HO phase (Figs. 4,8). A second, larger hole-like pocket is also centered on $\mathbf{Z}$ [25, 55] with $k_F \approx 0.4$ r.l.u. along $\mathbf{\Gamma}$-$\mathbf{Z}$. Remarkably, the extent of this pocket is nearly identical to the trough of inelastic magnetic scattering (Fig. 3), which forms a ring of overdamped magnetic scattering at high temperatures (Fig. 8). In contrast, there are no particularly strong signatures localized at these $q$ values in the phonon dispersions. Rather, the unusual temperature dependence of the optic modes extends along most of $\mathbf{\Gamma}$-$\mathbf{\Sigma}$ (Fig. 9). The large extent in reciprocal space may be associated with a possible third Fermi-level crossing along $\mathbf{\Gamma}$-$\mathbf{Z}$ with even larger $k_F$ [25, 55], but the full shape and extent of an associated pocket is unresolved in ARPES.

At the other high-symmetry points, the presence of Fermi level crossings is not obvious. We first address the $\mathbf{X}$ point, which harbors well-defined small square hole-like pockets [55] that have since been attributed to surface states [63]; soft x-ray ARPES also shows no intensity at $\mathbf{X}$ [25]. This is consistent with our measurements: the phonons do not exhibit any anomalous

temperature dependence at **X**, and while magnetic excitations in the HO phase are well-defined, they sit at relatively high $E$ and lack intensity compared to the excitations at **Z** and **Σ**. Meanwhile, the presence of a pocket at **Γ** is dubious, but less clear. It is not evident at 20 K in the bulk-sensitive soft x-ray ARPES [25], but it has been reported in multiple studies based on less-penetrating lower-energy ARPES measurements. In contrast to first-principles calculations predicting that this pocket is electron-like [55, 56] experiments suggest that it is actually hole-like, with $k_F \approx 0.2$ Å$^{-1}$ and an almost identical dispersion to that of the small pocket at **Z**, leading to interpretations of zone-folding [59, 60]. Our inelastic neutron and x-ray data concur with the bulk-sensitive ARPES; there are no phonon anomalies, nor are magnetic excitations discernable at these $q$ values (Fig. 3).

Altogether, the reciprocal-space correspondence between the magnetic excitations and two well-defined **Z**-centered hole pockets is striking (Fig.12). Moreover, these two pockets can account for the bulk transport data. The small hole pocket matches the dimensions of the $\alpha$ pocket measured by quantum oscillations [65] with an approximate carrier density of $2 \times 10^{20}$ cm$^{-3}$, which agrees well with the effective Hall carrier density in the HO phase [66]. The bigger pocket, which is not observed in quantum oscillations [65, 67–70], has a carrier density of order $10^{21}$ cm$^{-3}$, which agrees well with the larger Hall carrier density at high temperatures [71]. The carrier density decrease and absence of this larger pocket in the HO phase suggests that this pocket is gapped by the transition - hence a magnetic and charge gap open at the same $q$. Note also that the Hall data can be ascribed entirely to two hole pockets without the need to invoke compensation. Beyond these pockets, quantum oscillations also detect smaller pockets [65, 70]. Based on the correspondence between magnetic excitation minima and the measured Fermi pockets at **Z**, we place the small $\beta$ pockets along **Γ**-**X** approximately 0.15 r.l.u. away from **X** at the magnetic dispersion minimum there (Fig. 12). This pocket may be responsible for the low-temperature $TO_1$ phonon softening along **Γ**-**X** (Fig. 9). With an effective mass of 25 times the bare electron mass, the bands making up this pocket are very flat and within 1 meV of the Fermi level, and ARPES may not resolve them.

ARPES further suggests that these pockets all coexist with a narrow $f$-state that sits just below the Fermi level [58, 60], which is consistent with the fractional $f$-count determined by electron energy loss spectroscopy [72]. Note that the FS based on Ref. [25] that matches our data agrees in detail with neither calculations that treat the $f$-electrons as primarily itinerant [22, 56] nor as localized [57]; the actual electronic state is intermediate.

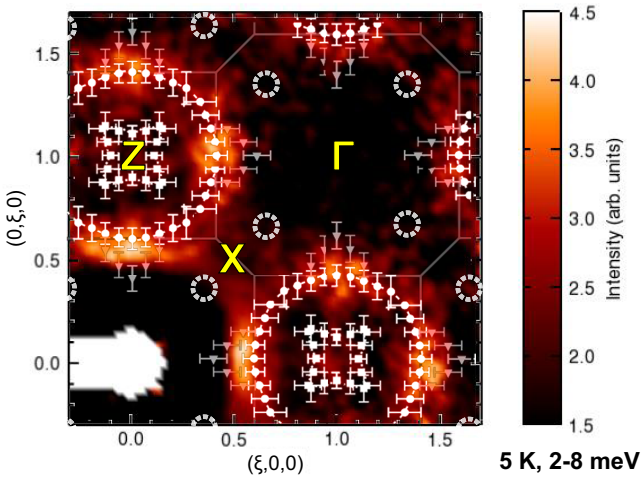


FIG. 12. Comparison of the integrated magnetic intensity, over 2-8 meV, in the HO phase to the Fermi surface. The magnetic excitations probed by inelastic neutron scattering appear to track the bulk Fermi surface in the paramagnetic phase as determined by soft x-ray ARPES (white points with error bars [25]). This agreement suggests that the magnetic scattering is due to excitations of the $f$-electrons into the conduction band. A likely location of additional Fermi pockets is at the dispersion minimum 0.15 r.l.u. away from **X** (dashed circles).

### Symmetry of the Hidden Order phase

Our data show that inside the HO phase, neither the lattice nor magnetic excitations show any overt sign of obeying ST symmetry. This can best be seen in Fig. 3, in which it is clear that the ST BZ overlaid over the magnetic dispersions is unrelated to the directionality of the magnetic dispersion (shown in simplified form in Fig. 13). Instead, the gapped magnetic excitations in the HO phase follow the same general shape as the overdamped modes do at high temperature in the BCT phase (Fig. 8).

The original reason for invoking ST symmetry in the HO phase was the inferred small-moment AFM order [8]. However, this scenario is experimentally discredited [10, 14–16, 73], and numerous studies have failed to find signs of any other candidate order parameters: spin density wave [31], charge density wave [7], and antiferroquadrupolar order [74] that could change translational symmetry. Careful comprehensive studies have also failed to find evidence for local rotational symmetry breaking on Ru and Si sites [75]. There are two remaining arguments in favor of ST symmetry of the HO phase. The first argument is that quantum oscillation frequencies do not change dramatically as pressure tunes the transition between HO and AFM phases. However, given the relatively small size of the detected FS cross-

sectional areas, it is likely that no large change would occur when the BCT BZ is reduced to ST, particularly if the larger pockets are centered on high-symmetry points as determined by ARPES (see Fig. 13). The second argument comes from recent ARPES studies, in which a flat M-shaped band hybridizes with a light hole-like band at $\mathbf{\Gamma}$ and $\mathbf{Z}$ below $T_{\rm HO}$ [59, 60], which is interpreted in the context of BZ folding. However, no hole-like band is observed at $\mathbf{\Gamma}$ in the more bulk-sensitive soft x-ray ARPES [25], and the possible role of surface states in the ARPES data still needs to be sorted out.

To contrast the electronic properties in the BCT and ST symmetries, it is instructive to consider the relationship between the HO and neighboring AFM phases. The first-order phase boundary separating them as a function of pressure [13, 73, 77, 78] originates from a significant reorganization of electronic states between the two. Such a transition is easier to reconcile with a change from BCT to ST symmetry between the HO and AFM phases, as opposed to a change of a complex electronic order parameter sharing the same spatial symmetry [20, 57]. A change in lattice symmetry also has important implications for the magnetic dispersions in the AFM phase, which should differ greatly from those in the HO phase. Because of the simple type A AFM structure, magnons would be expected to emanate from the magnetic reciprocal lattice point at $\mathbf{Z}$, reach a maximum energy at (0.5,0,0) and disperse downward to $\mathbf{\Gamma}$, although the intensity would drop dramatically in the first BZ due to the AFM structure factor (Fig. 13). Further, the excitation minimum at $\mathbf{\Sigma}$ would have to essentially disappear for the magnetic dispersion to respect mirror symmetry at the new zone boundary at (0.5,0,0). Indeed, this simple picture is consistent with the finding that under pressure, the excitation at $\mathbf{\Sigma}$ increases to 8 meV, while the gap at $\mathbf{Z}$ closes [79, 80]. Meanwhile, the FS properties remain relatively similar between the two phases, as the BZ folding does not change the FS cross-sections (Fig. 13) and the experimental similarity of the electrical resistivity and thermodynamic anomalies implies a reduction in charge carriers in both phases.

The possibility of incommensurate order, in particular in the context of nested FS pockets, remains a popular theme. However, compared to archetypes such as the charge density wave in uranium [81] and the spin density wave in chromium [49], $URu_2Si_2$ lacks a crucial characteristic, namely diffraction peaks, in nuclear, magnetic, or electronic scattering at any known incommensurate wavevector. Our data further show that there are no clear anomalies in the lattice or magnetic excitations that suggest an instability towards density-wave order. Positing an order parameter that does not couple to existing scattering probes circumvents these difficulties, but does not address the details of the prominent magnetic spectrum.

There have been several reports recently about square symmetry breaking in the basal plane that might be associated with electronic nematicity [23, 24]. In particular, torque magnetometry tracks an order-parameter-like signal with two-fold rotational symmetry, but in small samples [19]. Recent NMR measurements indicate that this signal is very small [76]. Cyclotron resonance measurements also suggest that there is basal-plane anisotropy in the electronic structure [47]. These findings are generally consistent with original identification via ultrasound of a softening in the $\Gamma_3$ mode below the coherence temperature [41]. The tendency towards orthorhombic distortion appears to be an underlying feature of the correlated paramagnetic phase that likely derives from the directionality of the constituent $f$-states. Its absence in high magnetic fields upon entry in to the polarized Fermi liquid phase [44] indicates that the existence of the HO phase relies on the electron correlations that set in at much higher temperatures. A structural or magnetic orthorhombic distortion would split the volume-averaged lattice or magnetic excitations, but this is not observed, which means that any associated $E$ and $q$ scales are rather small.

It should also be noted that the tendency towards AFM upon suppression of HO is not universal [82, 83]. Upon Re substitution, $T_{\rm HO}$ is suppressed [84], and beyond a critical concentration, ferromagnetic (FM) order emerges [51]. The electrons remain correlated and appear to defy Fermi liquid theory [85, 86], further manifested as unconventional magnetic critical scaling near the quantum transition separating the HO and FM phases [87]. Recent inelastic neutron scattering measurements show that the HO transitions towards FM order gradually: the excitations at $\mathbf{\Sigma}$ persist, while those at $\mathbf{Z}$ are weakened [34]. This proximate instability of the correlated state to FM order highlights that there are incipient $Q = 0$ correlations in $URu_2Si_2$ as well.

### Instability of the correlated state

In $URu_2Si_2$, electronic correlations are already evident at 300 K. The bulk magnetic susceptibility and electrical resistivity are noticeably directional, with an Ising anisotropy inherited from the uranium $f$-states. The basal-plane electrical resistivity has a negative temperature derivative between 80 K and at least 1,200 K [71], meaning that anomalous scattering exists over a very large temperature range. Down to temperatures of approximately 100 K, the easy-axis magnetic susceptibility is well-described by a Curie-Weiss law that reflects a full free-ion, weakly correlated uranium moment. Within the context of a single-ion Kondo scattering mechanism, wherein the uranium ions do not interact strongly with each other, this implies a very large Kondo temperature $T_K > 350$ K [71]. At the Fermi level, single-ion Kondo hybridization introduces a broad resonance of width $\sim$ 30 meV. As the correlations strengthen slowly upon cool-

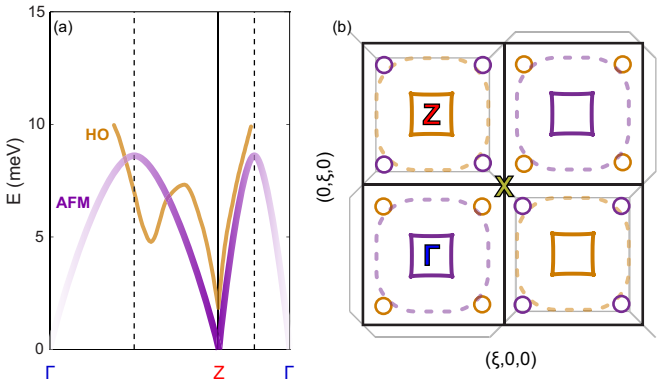


FIG. 13. Schematic comparison of HO/BCT and AFM/ST symmetries. a) The magnetic excitations in the HO phase (orange) do not observe the mirror symmetry required by the ST BZ boundaries (vertical dashed lines), whereas the AFM excitations (purple) should; these curves are based upon limited data under pressure [79, 80]. b) Comparison of the FS pockets in the BCT (orange) and ST (orange+purple) lattices in the basal plane. In the latter, the **Γ** and **Z** points become equivalent, changing the BZ boundaries from light gray to black. Considering the FS pocket assignments described in the text, the zone folding does *not* change the extremal cross-sections. The dashed FS pocket is gapped in the HO phase and presumably in the AFM phase.

ing, inter-ion effects strengthen and the Kondo resonance starts to form into a coherent band, but this occurs over a broad temperature range. The overdamped magnetic excitations detected in our study reveal that these correlations are strongest in well-defined parts of the BZ, tracing the FS contours detected by bulk-sensitive ARPES. In addition, ARPES confirms flat bands that are broad and incoherent in the vicinity of strongly dispersing $d$-states [58]. The overlap of the magnetic excitations and the FS pockets is highly unusual, and suggests that these magnetic excitations are signatures of the coupling of the hybridized $f$-state to the itinerant $d$-bands.

Only near 30 K, energy gaps are detected in point-contact spectroscopy (12 meV) [6], optical conductivity (10 meV) [4], photoinduced reflectivity [88], and nuclear magnetic resonance [89]. The multiple FS pockets of $URu_2Si_2$ can in principle support two energy gaps with different temperature evolution, and our study provides clues regarding how this occurs. Because the energy gap opening at $T_{HO}$ affects the large **Z**-centered hole pocket (as discussed above, refer to Fig. 13), the 30 K gap involves other itinerant electrons, namely the small FS pockets along **Γ**-**X** (Fig. 12), which have the heaviest measured mass at low temperatures. The high-temperature coherence energy scale and the 10 meV energy gaps, which are comparable to the magnetic excitation energy near **X**, are characteristics of the hybridization involving these small pockets. Since the FS pocket survives to low temperatures to be detected by quantum oscillations, the hybridization gap must sit at energies above the Fermi level. Thus, the measured magnetic form factor anisotropy in the HO phase (Fig. 6) ultimately reflects anisotropic $f$-$d$ hybridization potentials.

Hybridization is only complete in the HO phase. The magnetic excitations that track the electron correlations evolve from being overdamped in $E$ and confined in $q$ to well-defined in $E$ and dispersing in $q$ in the HO phase, yet they still trace the paramagnetic Fermi surface. The appearance of gaps in the magnetic excitations signals an additional, abrupt change at $T_{HO}$ in the electron correlations associated with the large **Z**-centered hole pocket (Fig. 13). Their presence accounts for the large entropy difference between the HO and high-temperature phases [30], the large reduction in quasiparticle scattering [46, 58], and the reduction in carrier concentration. This situation contrasts markedly with the case of nested FS sheets experiencing spin density wave order, which results in magnetic diffraction and sharply dispersive excitations localized in $q$ [90], even when the transition is suppressed [91]. The end result of the electronic reconstruction is that the small **Z**-centered FS pocket survives to dominate the electronic properties. Presumably, these carriers are finally responsible for superconductivity, which could explain why that phase does not coexist with the pressure-induced AFM phase [13].

How does the HO transition open additional energy gaps in the correlated electronic state? Our study clearly shows that there is no BCT symmetry-breaking involved in the HO phase transition, so BZ folding is not a mechanism that can be invoked; in fact, given the FS pocket locations, reduction to ST symmetry does not seem capable of gapping the FS either (Fig. 13). There is a large uranium $f$-state degeneracy - no experimental evidence shows that it is lifted appreciably by crystalline electric field effects - and Kondo hybridization introduces a large electronic DOS near the Fermi level. However, hybridization gaps open anisotropically: one at high temperature has the gentle temperature-dependence expected, but a second gap opens at the well-defined $T_{HO}$. This suggests that the hybridization of the correlated state changes in the HO phase, tracking an order parameter. To maintain BCT symmetry, any order parameter involving $f$-states has to resemble *ferro*-multipolar $Q = 0$ order because there is only one uranium atom per unit cell. It is tempting to label such a transition in terms of orbital ordering, but a full description must take into account the many-body nature of the renormalized $f$-state at low temperatures. The itineracy of this state explains the unusually low entropy associated with the transition itself (Fig. 11), and lies at the heart of what makes the phenomenology of $URu_2Si_2$ so unique. The HO transition facilitates a second hybridization of an already-hybridized band. Unlike the many examples of magnetic order in heavy fermion materials, HO is a nonmagnetic order that breaks the heavy fermion state.

### Conclusion

We have shown that the magnetic and lattice excitations in $URu_2Si_2$ obey the high-temperature body-centered tetragonal symmetry in the Hidden Order phase. The anisotropy of the magnetic form factor and the temperature-dependence of the magnetic excitations suggest that electron correlations in this material follow a two-step hybridization process, one with gradual temperature dependence, and the other that turns on at $T_{\rm HO}$, which appear to arise from different parts of the Brillouin zone. The magnetic excitations also exhibit a striking resemblance to the ARPES-determined Fermi surface, which underscores their identification with strong electron correlations, rather than elementary excitations due to long-range magnetic order or some kind of density wave order. Both of these are excluded from consideration due to a lack of elastic scattering, as well as no indication of mode softening in the inelastic scattering. The lack of evidence for simple tetragonal symmetry further excludes localized antiferromultipolar order, in favor of a ferro-type order parameter, although we suggest that a full theoretical description will require properly accounting for the many-body nature of the hybridized state.

### Acknowledgments

We would like to thank J. W. Allen, P. Chandra, P. Coleman, J. A. Mydosh, P. M. Oppeneer, T. Shibauchi, F. Weber, C. M. Varma, and T. Yanagisawa for valuable discussions and F. Bourdarot for sharing his unpublished data. We are particularly grateful to J. D. Denlinger for sharing his unpublished data and insight over the course of this study. NPB acknowledges support by CNAM and the LLNL PLS directorate. MEM was sponsored in part by the U.S. Department of Energy, Office of Basic Energy Sciences, Materials Sciences and Engineering Division. JRJ is partially supported by the Science Campaign. MJ gratefully acknowledges support by the Alexander von Humboldt Foundation. Portions of this work were performed under LDRD (Tracking Code 14-ERD-041). This work utilized facilities supported in part by the National Science Foundation under Agreement No. DMR-0944772. Use of the Advanced Photon Source, an Office of Science User Facility operated for the U.S. Department of Energy (DOE) Office of Science by Argonne National Laboratory, was supported by the U.S. DOE under Contract No. DE-AC02-06CH11357. LLNL is operated by Lawrence Livermore National Security, LLC, for the DOE, NNSA under Contract No. DE-AC52-07NA27344. Crystal growth at UCSD was supported by the U.S. DOE Grant No. DE-FG02-04ER46105.

* nicholas.butch@nist.gov

[1] T. T. M. Palstra, A. A. Menovsky, J. van den Berg, A. J. Dirkmaat, P. H. Kes, G. J. Nieuwenhuys, and J. A. Mydosh, "Superconducting and Magnetic Transitions in the Heavy-Fermion System $URu_2Si_2$," Phys. Rev. Lett. **55**, 2727 (1985).

[2] M. B. Maple, J. W. Chen, Y. Dalichaouch, T. Kohara, C. Rossel, M. S. Torikachvili, M. W. McElfresh, and J. D. Thompson, "Partially Gapped Fermi Surface in the Heavy-Electron Superconductor $URu_2Si_2$," Phys. Rev. Lett. **56**, 185 (1986).

[3] W. Schlabitz, J. Baumann, B. Pollit, U. Rauchschwalbe, H. M. Mayer, U. Ahlheim, and C. D. Bredl, "Superconductivity and Magnetic Order in a Strongly Interacting Fermi-System: $URu_2Si_2$," Z. Phys. B **62**, 171 (1986).

[4] J. Levallois, F. Lévy-Bertrand, M. K. Tran, D. Stricker, J. A. Mydosh, Y.-K. Huang, and D. van der Marel, "Hybridization gap and anisotropic far-infrared optical conductivity of $URu_2Si_2$." Phys. Rev. B **84**, 184420 (2011).

[5] P. Aynajian, E. H. da Silva Neto, C. V. Parker, Y. Huang, A. Pasupathy, J. Mydosh, and A. Yazdani, "Visualizing the formation of the Kondo lattice and the hidden order in $URu_2Si_2$," Proc. Natl. Acad. Sci. **107**, 10383 (2010).

[6] W. K. Park, P. H. Tobash, F. Ronning, E. D. Bauer, J. L. Sarrao, J. D. Thompson, and L. H. Greene, "Observation of the Hybridization Gap and Fano Resonance in the Kondo Lattice $URu_2Si_2$," Phys. Rev. Lett. **108**, 246403 (2012).

[7] A. R. Schmidt, M. H. Hamidian, P. Wahl, F. Meier, A. V. Balatsky, J. D. Garrett, T. J. Williams, G. M. Luke, and J. C. Davis, "Imaging the Fano lattice to 'hidden order' transition in $URu_2Si_2$," Nature **465**, 570 (2010).

[8] C. Broholm, J. K. Kjems, W. J. L. Buyers, P. Matthews, T. T. M. Palstra, A. A. Menovsky, and J. A. Mydosh, "Magnetic Excitations and Ordering in the Heavy-Electron Superconductor $URu_2Si_2$," Phys. Rev. Lett. **58**, 1467 (1987).

[9] H. Amitsuka, M. Yokoyama, S. Miyazaki, K. Tenya, T. Sakakibara, W. Higemoto, K. Nagamine, K. Matsuda, Y. Kohori, and T. Kohara, "Hidden order and weak antiferromagnetism in $URu_2Si_2$," Physica B 312-313, 390 (2002).

[10] S. Takagi, S. Ishihara, S. Saitoh, H.-I. Sasaki, H. Tanida, M. Yokoyama, and H. Amitsuka, "No Evidence for Small-Moment Antiferromagnetism under Ambient Pressure in $URu_2Si_2$: Single-Crystal $^{29}$Si NMR Study," J. Phys. Soc. Jpn. 76, 033708 (2007).

[11] H. Amitsuka, M. Sato, N. Metoki, M. Yokoyama, K. Kuwahara, T. Sakakibara, H. Morimoto, S. Kawarazaki, Y. Miyako, and J. A. Mydosh, "Effect of Pressure on Tiny Antiferromagnetic Moment in the Heavy-Electron Compound $URu_2Si_2$,"Phys. Rev. Lett. **83**, 5114 (1999).

[12] K. Matsuda, Y. Kohori, T. Kohara, K. Kuwahara and H. Amitsuka, "Spatially Inhomogeneous Development of Antiferromagnetism in $URu_2Si_2$: Evidence from $^{29}$Si NMR under Pressure," Phys. Rev. Lett. **87**, 087203 (2001).

[13] N. P. Butch, J. R. Jeffries, S. Chi, J. B. Leão, J. W. Lynn, and M. B. Maple, "Antiferromagnetic critical pressure in $URu_2Si_2$ under hydrostatic conditions." Phys. Rev. B 82, 060408 (2010).

[14] P. Das, R. E. Baumbach, K. Huang, M. B. Maple, Y. Zhao, J. S. Helton, J. W. Lynn, E. D. Bauer, and M. Janoschek, "Absence of a static in-plane magnetic moment in the hidden-order phase of $URu_2Si_2$," New J. Phys. 15, 053031 (2013)

[15] N. Metoki, H. Sakai, E. Yamamoto, N. Tateiwa, T. Matsuda, and Y. Haga, "Neutron Scattering Experiments for the Study of In-Plane Ordered Moment in $URu_2Si_2$," J. Phys. Soc. Jpn. 82, 055004 (2013)

[16] K. A. Ross, L.Harriger, Z. Yamani, W. J. L. Buyers, J. D. Garrett, A. A. Menovsky, J. A. Mydosh, and C. L. Broholm, "Strict limit on in-plane ordered magnetic dipole moment in $URu_2Si_2$," arXiv:1402.2689v1.

[17] N. Kernavanois, P. Dalmas de Réotier, A. Yaouanc, J.-P. Sanchez, K. D. Liß, P. Lejay, "Investigation of the crystal structure of $URu_2Si_2$ by high-resolution X-ray diffraction," Physica B 259-261, 648 (1999).

[18] J.-Q. Meng, P. M. Oppeneer, J. A. Mydosh, P. S. Riseborough, K. Gofryk, J. J. Joyce, E. D. Bauer, Y. Li, and T. Durakiewicz, "Imaging the Three-Dimensional Fermi-Surface Pairing near the Hidden-Order Transition in $URu_2Si_2$ Using Angle-Resolved Photoemission Spectroscopy," Phys. Rev. Lett. 111, 127002 (2013).

[19] R. Okazaki, T. Shibauchi, H. J. Shi, Y. Haga, T. D. Matsuda, E. Yamamoto, Y. Onuki, H. Ikeda, and Y. Matsuda, "Rotational Symmetry Breaking in the Hidden-Order Phase of $URu_2Si_2$," Science 331, 439 (2011).

[20] P. Chandra, P. Coleman, and R. Flint, "Hastatic order in the heavy-fermion compound $URu_2Si_2$," Nature 493, 612 (2013)

[21] H. Harima, K. Miyake, and J. Flouquet, "Why the Hidden Order in $URu_2Si_2$ Is Still HiddenOne Simple Answer," J. Phys. Soc. Jpn. 79, 033705 (2010)

[22] P. M. Oppeneer, J. Rusz, S. Elgazzar, M.-T. Suzuki, T. Durakiewicz, and J. A. Mydosh, "Electronic structure theory of the hidden-order material $URu_2Si_2$." Phys. Rev. B 82, 205103 (2010).

[23] S. Fujimoto, "Spin Nematic State as a Candidate of the Hidden Order Phase of $URu_2Si_2$." Phys. Rev. Lett. 106, 196407 (2011).

[24] H. Ikeda, M. Suzuki, R. Arita, T. Takimoto, T. Shibauchi, and Y. Matsuda, "Emergent rank-5 nematic order in $URu_2Si_2$," Nature Phys. 8, 528 (2012).

[25] I. Kawasaki, S. Fujimori, Y. Takeda, T. Okane, A. Yasui, Y. Saitoh, H. Yamagami, Y. Haga, E. Yamamoto, and Y. Onuki, "Band structure and Fermi surface of $URu_2Si_2$ studied by soft x-ray angle-resolved photoemission spectroscopy." Phys. Rev. B 83, 235121 (2011).

[26] J. W. Lynn, Y. Chen, S. Chang, Y. Zhao, S. Chi, W. Ratcliff, II, B. G. Ueland, and R. W. Erwin, "Double Focusing Thermal Triple Axis Spectrometer at the NCNR," J. Res. Natl. Inst. Stan. Technol. 117, 61-79 (2012).

[27] W. C. Chen, T. R. Gentile, C. B. Fu, S. Watson, G. L. Jones, J. W. McIver, and D. R. Rich,"Polarized $^3$He cell development and application at NIST," J. Phys.: Conf. Ser. 294, 012003 (2011).

[28] J. R. D. Copley and J. C. Cook, "The Disk Chopper Spectrometer at NIST: a new instrument for quasielastic neutron scattering studies", Chem. Phys. 292, 477 (2003).

[29] R. T. Azuah, L. R. Kneller, Y. Qiu, P. L. W. Tregenna-Piggott, C. M. Brown, J. R. D. Copley, and R. M. Dimeo, "DAVE: A comprehensive software suite for the reduction, visualization, and analysis of low energy neutron spectroscopic data", J. Res. Natl. Inst. Stan. Technol. 114, 341 (2009).

[30] C. R. Wiebe, J. A. Janik, G. J. MacDougall, G. M. Luke, J. D. Garrett, H. D. Zhou, Y.-J. Jo, L. Balicas, Y. Qiu, J. R. D. Copley, Z. Yamani, and W. J. L. Buyers, "Gapped itinerant spin excitations account for missing entropy in the hidden-order state of $URu_2Si_2$." Nature Phys. 3, 96 (2007).

[31] W. J. L. Buyers, "Low moments in heavy-fermion systems," Physica B 223&224, 9 (1996).

[32] C. Broholm, H. Lin, P. T. Matthews, T. E. Mason, W. J. L. Buyers, M. F. Collins, A. A. Menovsky, J. A. Mydosh, and J. K. Kjems, "Magnetic excitations in the heavy-fermion superconductor $URu_2Si_2$," Phys. Rev. B 43, 12809 (1991).

[33] F. Bourdarot, A. Bombardi, P. Burlet, M. Enderle, J. Flouquet, P. Lejay, N. Kernavanois, V. P. Mineev, L. Paolasini, M. E. Zhitomirsky, and B. Fåk, "Hidden order in $URu_2Si_2$," Physica B **359-361**, 986 (2005).

[34] T. J. Williams, Z. Yamani, N. P. Butch, G. M. Luke, M. B. Maple, and W. J. L. Buyers, "Neutron scattering study of $URu_{2-x}Re_xSi_2$ (x = 0.10): Driving order towards quantum criticality," Phys. Rev. B 86, 235104 (2012)

[35] P. Chandra, P. Coleman, J. A. Mydosh and V. Tripathi, "Hidden orbital order in the heavy fermion metal $URu_2Si_2$," Nature 417, 831 (2002).

[36] C. R. Wiebe, G. M. Luke, Z. Yamani, A. A. Menovsky, and W. J. L. Buyers, "Search for hidden orbital currents and observation of an activated ring of magnetic scattering in the heavy fermion superconductor $URu_2Si_2$," Phys. Rev. B 69, 132418 (2004)

[37] K. Kuwahara, M. Kohgi, K. Iwasa, M. Nishi, K. Nakajima, M. Yokoyama, H. Amitsuka, "Magnetic form factor of $URu_2Si_2$," Physica B 378-380, 581 (2006)

[38] R. M. Moon, "Spin densities and form factors: past, present, and future," Physica 137B, 19-30 (1986).

[39] J. W. Lynn, G. Shirane, and M. Blume, "Covalency effects in the magnetic form factor of Ir in $K_2IrCl_6$," Phys. Rev. Lett. 37, 154-157 (1976).

[40] A. C. Walters, T. G. Perring, J.-S. Caux, A. T. Savici, G. D. Gu, C.-C. Lee, W. Ku, and I. A. Zaliznyak, "Effect of covalent bonding on magnetism and the missing neutron intensity in copper oxide compounds," Nature Phys. 5, 867 (2009).

[41] K. Kuwahara, A. Amitsuka, T. Sakakibara, O. Suzuki, S. Nakamura, T. Goto, M. Mihalik, A. A. Menovsky, A. de Visser, and J. J. M. Franse, "Lattice Instability and Elastic Response in the Heavy Electron System $URu_2Si_2$," J. Phys. Soc. Jpn. 66, 3251 (1997).

[42] S. L. Cooper, M. V. Klein, M. B. Maple, and M. S. Torikachvilli, "Magnetic exctitations and phonon anomalies in $URu_2Si_2$," Phys. Rev. B 36, 5743 (1987).

[43] D. Lampakis, D. Palles, E. Liarokapis, and J. A. Mydosh, "Raman study of the heavy fermion system $URu_2Si_2$ at low temperatures and high hydrostatic pressures," Physica B 378380, 578 (2006).

[44] T. Yanagisawa, S. Mombetsu, H. Hidaka, H. Amitsuka, M. Akatsu, S. Yasin, S. Zherlitsyn, J. Wosnitza, K. Huang, and M. B Maple, "Hybridization-driven orthorhombic lattice instability in $URu_2Si_2$," Phys. Rev. B 88, 195150 (2013).

[45] K. Behnia, R. Bel, Y. Kasahara, Y. Nakajima, H. Jin, H. Aubin, K. Izawa, Y. Matsuda, J. Flouquet, Y. Haga, Y.

Onuki, and P. Lejay, "Thermal Transport in the Hidden-Order State of $URu_2Si_2$," Phys. Rev. Lett. **94**, 156405 (2005).

[46] P. A. Sharma, N. Harrison, M. Jaime, Y. S. Oh, K. H. Kim, C. D. Batista, H. Amitsuka, and J. A. Mydosh, "Phonon Thermal Transport of $URu_2Si_2$: Broken Translational Symmetry and Strong-Coupling of the Hidden Order to the Lattice," Phys. Rev. Lett. **97**, 156401 (2006).

[47] S. Tonegawa, K. Hashimoto, K. Ikada, Y.-H. Lin, H. Shishido, Y. Haga, T. D. Matsuda, E. Yamamoto, Y. Onuki, H. Ikeda, Y. Matsuda, and T. Shibauchi, "Cyclotron Resonance in the Hidden-Order Phase of $URu_2Si_2$." Phys. Rev. Lett. 109, 036401 (2012).

[48] J. W. L. Pang, W. J. L. Buyers, A. Chernatynskiy, M. D. Lumsden, B. C. Larson, and S. R. Phillpot, "Phonon Lifetime Investigation of Anharmonicity and Thermal Conductivity of $UO_2$ by Neutron Scattering and Theory," Phys. Rev. Lett. 110, 157401 (2013).

[49] E. Fawcett, "Spin-density-wave antiferromagnetism in chromium." Rev. Mod. Phys. 60, 209 (1988).

[50] J.-G. Park, K. A. McEwen, and M. J. Bull, "High-energy magnetic excitations of $URu_2Si_2$," Phys. Rev. B 66, 094502 (2002)

[51] N. P. Butch and M. B. Maple, "The suppression of hidden order and the onset of ferromagnetism in $URu_2Si_2$ via Re substitution," J. Phys. Condens. Matter 22, 164204 (2010)

[52] T. Yamashita, S. Tonegawa, Y. Tsuruhara, H. Sumiyoshi, S. Fujimoto, T. Matsuda, Y. Haga, E. Yamamoto, Y. Onuki, T. Shibauchi, and Y. Matsuda, "Anomalous Nernst effect of the heavy-fermion superconductor $URu_2Si_2$," APS March Meeting 2014.

[53] A. V. Balatsky, A. Chantis, H. P. Dahal, D. Parker, and J. X. Zhu, "Incommensurate spin resonance in $URu_2Si_2$," Phys. Rev. B 79, 214413 (2009)

[54] J. A. Janik, H. D. Zhou, Y.-J. Jo, L. Balicas, G. J. MacDougall, G.M. Luke, J. D. Garrett, K. J. McClellan, E. D. Bauer, J. L. Sarrao, Y. Qiu, J. R. D. Copley, Z. Yamani, W. J. L. Buyers, and C. R. Wiebe, "Itinerant spin excitations near the hidden order transition in $URu_2Si_2$," J. Phys. Condens. Matter 21, 192202 (2009).

[55] J. D. Denlinger, G.-H. Gweon, J. W. Allen, C. G. Olson, M. B. Maple, J. L. Sarrao, P. E. Armstrong, Z. Fisk, and H. Yamagami, "Comparative study of the electronic structure of $XRu_2Si_2$: probing the Anderson lattice." J. Electron Spectrosc. 117-118, 347 (2001).

[56] S. Elgazzar, J. Rusz, M. Amft, P. M. Oppeneer, and J. A. Mydosh, "Hidden order in $URu_2Si_2$ originates from Fermi surface gapping induced by dynamic symmetry breaking," Nature Mat. 8, 337 (2009)

[57] K. Haule, and G. Kotliar, "Arrested Kondo effect and hidden order in $URu_2Si_2$," Nature Phys. 5, 796 (2009).

[58] S. Chatterjee, J. Trinckauf, T. Hänke, D. E. Shai, J. W. Harter, T. J. Williams, G. M. Luke, K. M. Shen, and J. Geck, "Formation of the Coherent Heavy Fermion Liquid at the Hidden Order Transition in $URu_2Si_2$," Phys. Rev. Lett. 110, 186401 (2013)

[59] R. Yoshida, K. Tsubota, T. Ishiga, M. Sunagawa, J. Sonoyama, D. Aoki, J. Flouquet, T. Wakita, Y. Muraoka, and T. Yokoya, "Translational Symmetry Breaking and Gapping of Heavy-Quasiparticle Pocket in $URu_2Si_2$," Sci. Rep. 3, 2750 (2013)

[60] F. L. Boariu, C. Bareille, H. Schwab, A. Nuber, P. Lejay, T. Durakiewicz, F. Reinert, and A. F. Santander-Syro, "Momentum-Resolved Evolution of the Kondo Lattice into Hidden Order in $URu_2Si_2$," Phys. Rev. Lett. 110, 156404 (2013)

[61] T. Ito, H. Kumigashira, T. Takahashi, Y. Haga, E. Yamamoto, T. Honma, H. Ohkuni, and Y. Ōnuki, "Band structure and Fermi surface of $URu_2Si_2$ studied by high-resolution angle-resolved photoemission spectroscopy," Phys. Rev. B 60, 13390 (1999)

[62] R. Yoshida, M. Fukui, Y. Haga, E. Yamamoto, Y. Onuki, M. Okawa, W. Malaeb, S. Shin, Y. Muraoka, and T. Yokoya, "Signature of hidden order and evidence for periodicity modification in $URu_2Si_2$," Phys. Rev. B 85, 241102(R) (2012)

[63] J. Denlinger, O. Krupin, J. W. Allen, B. J. Kim, K. Haule, K. Kim, G. Kotliar, J. L. Sarrao, N. P. Butch, and M. B. Maple, "Quantification of U f-valence in $URu_2Si_2$ from 3D Bulk Fermi Surface Topology," APS March Meeting 2011.

[64] A. F. Santander-Syro, M. Klein, F. L. Boariu, A. Nuber, P. Lejay, and F. Reinert, "Fermi-surface instability at the hidden-order transition of $URu_2Si_2$," Nature Phys. 5, 637 (2009)

[65] E. Hassinger, G. Knebel, T. D. Matsuda, D. Aoki, V. Taufour, and J. Flouquet, "Similarity of the Fermi Surface in the Hidden Order State and in the Antiferromagnetic State of $URu_2Si_2$." Phys. Rev. Lett. 105, 216409 (2010).

[66] Y. Kasahara, T. Iwasawa, H. Shishido, T. Shibauchi, K. Behnia, Y. Haga, T. D. Matsuda, Y. Onuki, M. Sigrist, and Y. Matsuda, "Exotic Superconducting Properties in the Electron-Hole-Compensated Heavy-Fermion Semimetal $URu_2Si_2$," Phys. Rev. Lett. **99**, 116402 (2007).

[67] M. Nakashima, H. Ohkuni, Y. Inada, R. Settai, Y. Haga, E. Yamamoto, and Y. Ōnuki, "The de Haasvan Alphen effect in $URu_2Si_2$ under pressure," J. Phys.: Condens. Matter **15**, S2011 (2003).

[68] Y. J. Jo, L. Balicas, C. Capan, K. Behnia, P. Lejay, J. Flouquet, J. A. Mydosh, and P. Schlottmann, "Field-Induced Fermi Surface Reconstruction and Adiabatic Continuity between Antiferromagnetism and the Hidden-Order State in $URu_2Si_2$," Phys. Rev. Lett. **98**, 166404 (2007).

[69] M. M. Altarawneh, N. Harrison, S. E. Sebastian, L. Balicas, P. H. Tobash, J. D. Thompson, F. Ronning, and E. D. Bauer, "Sequential Spin Polarization of the Fermi Surface Pockets in $URu_2Si_2$ and Its Implications for the Hidden Order," Phys. Rev. Lett. 106, 146403 (2011)

[70] H. Ohkuni, Y. Inada, Y. Tokiwa, K. Sakurai, R. Settai, T. Honma, Y. Haga, E. Yamamoto, Y. Onuki, H. Yamagami, S. Takahashi, and T. Yanagisawa, "Fermi surface properties and de Haas van Alphen oscillation in both the normal and superconducting mixed states of $URu_2Si_2$," Phil. Mag. B 79, 1045 (1999)

[71] J. Schoenes, C. Schönenberger, J. J. M. Franse, and A. A. Menovksky, "Hall-effect and resistivity study of the heavy-fermion system $URu_2Si_2$," Phys. Rev. B 35, 5375 (1987)

[72] J. R. Jeffries, K. T. Moore, N. P. Butch, and M. B. Maple, "Degree of 5f electron localization in $URu_2Si_2$: Electron energy-loss spectroscopy and spin-orbit sum rule analysis." Phys. Rev. B 82, 033103 (2010).

[73] H. Amitsuka, K. Matsuda, I. Kawasaki, K. Tenya, M. Yokoyama, C. Sekine, N. Tateiwa, T. C. Kobayashi, S. Kawarazaki, and H. Yoshizawa, "Pressuretemperature phase diagram of the heavy-electron superconductor $URu_2Si_2$," J. Magn. Magn. Mater. **310**, 214 (2007).

[74] H. Amitsuka, T. Inami, M. Yokoyama, S. Takayama, Y. Ikeda, I. Kawasaki, Y. Homma, H. Hidaka, and T. Yanagisawa, "Resonant X-ray scattering study of hidden order in $URu_2Si_2$ using a low-stress single crystal," J. Phys. Conf. Series 200, 012007 (2010).

[75] T. Mito, M. Hattori, G. Motoyama, Y. Sakai, T. Koyama, K. Ueda, T. Kohara, M. Yokoyama, and H.i Amitsuka, "Investigation of Local Symmetries in the Hidden-Order Phase of $URu_2Si_2$," J. Phys. Soc. Jpn. 82, 123704 (2013).

[76] S. Kambe, Y. Tokunaga, H. Sakai, T. D. Matsuda, Y. Haga, Z. Fisk, and R. E. Walstedt, "NMR Study of In-Plane Twofold Ordering in $URu_2Si_2$,"Phys. Rev. Lett. 110, 246406 (2013).

[77] H. Amitsuka, K. Tenya, M. Yokoyama, A. Schenck, D. Andreica, F. N. Gygax, A. Amato, Y. Miyako, Y. K. Huang, J. A. Mydosh, "Inhomogeneous magnetism in $URu_2Si_2$ studied by muon spin relaxation under high pressure," Physica B **326**, 418 (2003).

[78] A. Amato, M. J. Graf, A. de Visser, H. Amitsuka, D. Andreica, and A. Schenck, "Weak-magnetism phenomena in heavy-fermion superconductors: selected $\mu$SR studies," J. Phys.: Condens. Matter **16**, S4403 (2004).

[79] A. Villaume, F. Bourdarot, E. Hassinger, S. Raymond, V. Taufour, D. Aoki, and J. Flouquet, "Signature of hidden order in heavy fermion superconductor $URu_2Si_2$: Resonance at the wave vector $Q_0 = (1, 0, 0)$." Phys. Rev. B 78, 012504 (2008).

[80] F. Bourdarot, E. Hassinger, S. Raymond, D. Aoki, V. Taufour, L.-P. Regnault, and Jacques Flouquet, "Precise Study of the Resonance at $Q_0 = (1, 0, 0)$ in $URu_2Si_2$," J. Phys. Soc. Jpn. 79, 064719 (2010)

[81] H. G. Smith and G. H. Lander, "Neutron scattering investigations of $\alpha$-uranium in the charge-density-wave state," Phys. Rev. B 30, 5407 (1984).

[82] Y. Dalichaouch, M. B. Maple, M. S. Torikachvili, and A. L. Giorgi, "Ferromagnetic instability in the heavy-electron compound $URu_2Si_2$ doped with Re or Tc," Phys. Rev. B **39**, 2423 (1989).

[83] Y. Dalichaouch, M. B. Maple, J. W. Chen, T. Kohara, C. Rossel, M. S. Torikachvili, and A. L. Giorgi, "Effect of transition-metal substitutions on competing electronic transitions in the heavy-electron compound $URu_2Si_2$," Phys. Rev. B **41**, 1829 (1990).

[84] J. R. Jeffries, N. P. Butch, B. T. Yukich, and M. B. Maple, "Competing Ordered Phases in $URu_2Si_2$: Hydrostatic Pressure and Rhenium Substitution," Phys. Rev. Lett. **99**, 217207 (2007).

[85] E. D. Bauer, V. S. Zapf, P.-C. Ho, N. P. Butch, E. J. Freeman, C. Sirvent, and M. B. Maple, "Non-Fermi-Liquid Behavior within the Ferromagnetic Phase in $URu_{2-x}Re_xSi_2$," Phys. Rev. Lett. 94, 046401 (2005)

[86] V. V. Krishnamurthy, D. T. Adroja, N. P. Butch, S. K. Sinha, M. B. Maple, R. Osborn, J. L. Robertson, S. E. Nagler, and M. C. Aronson, "Magnetic short-range correlations and quantum critical scattering in the non-Fermi liquid regime of $URu_{2-x}Re_xSi_2$ $(x = 0.2 - 0.6)$," Phys. Rev. B **78**, 024413 (2008).

[87] N. P. Butch and M. B. Maple, "Evolution of Critical Scaling Behavior near a Ferromagnetic Quantum Phase Transition," Phys. Rev. Lett. 103, 076404 (2009)

[88] M. K. Liu, R. D. Averitt, T. Durakiewicz, P. H. Tobash, E. D. Bauer, S. A. Trugman, A. J. Taylor, and D. A. Yarotski, "Evidence of a hidden-order pseudogap state in $URu_2Si_2$ using ultrafast optical spectroscopy," Phys. Rev. B 84, 161101(R) (2011)

[89] K. R. Shirer, J. T. Haraldsen, A. P. Dioguardi, J. Crocker, N. apRoberts-Warren, A. C. Shockley, C.-H. Lin, D. M. Nisson, J. C. Cooley, M. Janoschek, K. Huang, N. Kanchanavatee, M. B. Maple, M. J. Graf, A. V. Balatsky, and N. J. Curro, "Nuclear magnetic resonance studies of pseudospin fluctuations in $URu_2Si_2$," Phys. Rev. B 88, 094436 (2013)

[90] Y. Endoh and P. Böni, "Magnetic Excitations in Metallic Ferro- and Antiferromagnets," J. Phys. Soc. Jpn. 75, 111002 (2006)

[91] E. Fawcett, H. L. Alberts, V. Yu. Galkin, D. R. Noakes, and J. V. Yakhmi, "Spin-density-wave antiferromagnetism in chromium alloys," Rev. Mod. Phys. 66, 25 (1994).